

October 9, 2018

THE PHYSICS OF A SEXTET QUARK SECTOR*

Alan. R. White[†]

Argonne National Laboratory
9700 South Cass, Il 60439, USA.

Abstract

Electroweak symmetry breaking may be a consequence of color sextet quark chiral symmetry breaking. A special solution of QCD is involved, with a high-energy S-Matrix that can be constructed “semi-perturbatively” via the chiral anomaly and reggeon diagrams. An infra-red fixed point and color superconductivity are crucial components of the construction. Infinite momentum physical states contain both quarks and a universal “anomalous wee gluon” component, and the spectrum is more limited than is required by confinement and chiral symmetry breaking. The pomeron is approximately a regge pole and the Critical Pomeron describes asymptotic cross-sections.

The strong coupling of the pomeron to the electroweak sector could produce large x and Q^2 events at HERA, and vector boson pairs at Fermilab. Further evidence for the sextet sector at Fermilab would be a large E_T jet excess, due in part to the non-evolution of α_s , and other phenomena related to the possibility that top quark production is due to the η_6 .

The sextet proton and neutron are the only new baryonic states. Sextet states dominate high energy hadronic cross-sections and stable sextet neutrons could produce both dark matter and ultra high energy cosmic rays. The cosmic ray spectrum knee suggests the effective sextet threshold is between Fermilab and LHC energies, with large cross-section effects expected at the LHC. Jet and vector boson cross-sections will be very much larger than expected, and sextet baryons should also be produced. Double pomeron produced states could provide definitive evidence for the existence of the sextet sector in the initial low luminosity running.

*Work supported by the U.S. Department of Energy under Contract W-31-109-ENG-38

[†]arw@hep.anl.gov

1. INTRODUCTION

The initial pursuit[1, 2], nearly thirty years ago, of a particular solution of supercritical Reggeon Field Theory (RFT) has led us to first associate the Critical Pomeron[3] with a special high-energy S-Matrix solution of QCD, then to connect this QCD solution to a very particular form of electroweak symmetry breaking[4, 5]. If this is the symmetry breaking and solution of QCD chosen by nature then, as outlined in [6], [7] and [8], we anticipate that there is a major change in the strong interaction above the electroweak scale. A new color sextet sector appears, with electroweak scale masses, that at high enough energies should become responsible for the major part of the total cross-section. The existence of this sector offers a natural explanation for the dominance of dark matter and in fact, an interaction change of just this kind could be responsible for the apparent “knee” in the cosmic ray spectrum that occurs just above the Tevatron energy. Other cosmic ray phenomena, that occur above the knee energy, also appear to be clear evidence for the same interaction change. That the knee is associated with the effective energy threshold for the sextet sector would be natural if inclusive pomeron exchange has to be involved when sextet states are produced, with large cross-section, from initial triplet states.

We should emphasize that it could be (even though we consider it unlikely) that the knee is not associated with sextet physics. If it is, however, then large cross-section effects have to appear very rapidly as the energy increases and they should be apparent at the LHC, with dramatic and exciting physics involved. In particular, jet cross-sections and electroweak vector boson cross-sections will be overwhelmingly large, with pomeron exchange cross-sections containing the most distinctive signals. Some indication of this physics could be observable at the Tevatron, or even at HERA. Hints of what is to come, that may already have been seen, could be the large E_T jet excess at the Tevatron and large x and Q^2 events at HERA.

We will use QCD_S to denote[‡] the S-Matrix solution of QCD with six color triplet and two color sextet quarks that we will describe. Within QCD_S , sextet chiral symmetry breaking gives a triplet of “sextet pions” (Π^\pm , Π^0) and also, at first sight, a “higgs-like” particle - the η_6 . When the electroweak sector of the Standard Model is added, the “sextet higgs mechanism” takes place. By “eating” the Π ’s, the W^\pm and Z^0 acquire masses that are a manifestation of the QCD sextet chiral scale. Thus, electroweak symmetry breaking is accomplished without any new interaction being added to the established $SU(3) \otimes SU(2) \otimes U(1)$ gauge interactions of the Standard Model. (We will only briefly discuss how an $SU(2) \otimes U(1)$ anomaly is avoided since

[‡]The suffix can be thought of as denoting “special”, or “sextet”, or “saturated” - the asymptotic freedom constraint is “saturated”. The “special” nature of the S-Matrix will become evident.

a special unification, requiring additional discussion, is most likely involved[9, 10].) Furthermore, the electroweak scale is a new QCD scale and the symmetry breaking is connected with the major change in the strong interaction discussed above.

We obtain the QCD_S high-energy S-Matrix via the powerful technology of reggeon diagrams[11]-[16]. While this S-Matrix has some important distinctive properties relative to conventional QCD, we believe that it is consistent with all the (experimentally established) properties of QCD below the electroweak scale. A crucial distinctive property is, however, the limitation on the spectrum of states compared to what would be anticipated from just color confinement and chiral symmetry breaking. As we will describe, the S-Matrix is constructed as a reggeon critical phenomenon by starting within a “color superconducting” phase of QCD_S (in which SU(3) color is broken to SU(2)). This starting point introduces reggeon “anomaly interactions” that are a key physical ingredient. These interactions produce divergences which have the consequence that the physical states of QCD_S are directly related to the chiral Goldstone bosons of the superconducting theory. This implies that, in the normal hadronic sector, both glueballs and quark resonances (such as the ρ) are directly excluded as asymptotic states.

In general, because of the central role played by anomaly couplings, only a very limited sub-set of the gluon degrees of freedom contribute to the QCD_S high-energy S-Matrix. (Presumably, there is a corresponding limitation in the finite energy S-Matrix.) As a result, there is no BFKL pomeron and no odderon. We are not aware of any experimental evidence against this. Rather, strong experimental evidence that this should be the case is, surely, provided by the (almost total) absence of glueballs in the resonance spectrum, the absence of the odderon[17] in experiments at HERA, and the lack[17] of any definitive evidence for the BFKL pomeron.

The spectrum of states involving sextet quarks is, perhaps, the deepest consequence of the construction of the spectrum of QCD_S via the anomaly interactions of the superconducting phase. Because there are no chiral symmetries linking the sextet and triplet quarks, there are no hybrid sextet/triplet states and the only new sextet states, in addition to the sextet pions and the η_6 , are a “sextet proton” (the P_6) and the “sextet neutron” (the N_6), both of which will have electroweak scale masses that could be, we will suggest, as low as 500 GeV . Because of the conservation of sextet quark baryon number, one of the sextet nucleons must be absolutely stable. The absence of sextet current quark masses (that is necessary for electroweak symmetry breaking) implies that the stable state must be the N_6 . Therefore, at the ultra-high energies relevant for the early universe, the production of stable, neutral, sextet neutrons will dominate over the production of stable, charged, triplet protons. Consequently, we have a very natural explanation for the dominance of dark matter - formed (as nuclei, clumps, etc.) from sextet neutrons. Furthermore, because neutral, massive, N_6 ’s will avoid the GZK cut-off they could also be the mysterious, ultra-high

energy, cosmic rays. Since they would simply be very high energy dark matter their origin would, presumably, be much less of a mystery than is currently believed.

The purpose of this paper is two-fold. Firstly, we want to lay out what we believe we know about QCD_S and why we think we know it. Secondly, we will outline experimental consequences that we expect from the combination of QCD_S with the sextet higgs mechanism. While we have discussed high-energy phenomena that QCD_S could produce in the past[18, 19], we did not have the detailed understanding that we now have of how the chiral anomaly produces high-energy states and amplitudes. As a result, the emphasis in this paper will be very different to that of our earlier papers[§]. Particularly important will be the strong coupling of the pomeron to sextet states that follows from the anomaly pole method that we develop to estimate cross-sections for hard diffraction. Predictions can then be made for soft diffraction by combining the hard diffractive estimates with pomeron regge theory.

If pomeron exchange amplitudes are large, then cut-pomeron amplitudes should also be large. This leads to the prediction of large inclusive cross-sections for sextet states (multiple W 's and Z 's, in particular) across most of the rapidity axis, that we expect to be the major characteristic of QCD_S physics above the electroweak scale. There will also be “non-diffractive” consequences of the sextet sector that we will discuss. At current energies, these include the non-evolution of α_s above the electroweak scale and the possibility that top production is due to the η_6 .

While our papers have suggested a link for some time, we believe that the arguments presented in this paper make it clear that the sextet higgs mechanism is inextricably tied to the pomeron and infinite momentum hadron states that have emerged from our work on the regge limit of QCD_S . If this were not the case then, as we discuss again below, the η_6 would be[20] a light axion-like state that is not seen experimentally and the sextet Higg's mechanism would be ruled out as a realistic possibility. We will emphasize (see Appendix C in particular) the likelihood that the left-handed vector nature of the electroweak sector of the Standard Model plays an important role with respect to inducing the special QCD_S S-Matrix.

That the high-energy behavior can be constructed by starting from the reggeon diagrams of $CSQCD_S$ (“color superconducting” QCD_S) is the most crucial property of QCD_S . The original motivation for this starting point came from a correspondence between supercritical pomeron RFT and $CSQCD_S$. This correspondence is referred to indirectly above and the arguments for it are described in Appendix C - where we outline our full multi-regge program. There is, however, an important technical reason why the construction can be carried through. $CSQCD_S$ can be obtained from QCD_S by introducing an asymptotically free scalar field. (This would not be possible if the number of quarks was any fewer!) Asymptotic freedom implies

[§]Most notably we believe our discussion of instanton interactions and dynamical masses is irrelevant in the, infinite momentum, S-Matrix formulation within which we now work.

that this field can be smoothly decoupled in the ultra-violet region. In the infra-red region the only remnant of the decoupling is the “anomaly contribution” of unphysical longitudinal wee gluons that provides the all important mechanism that produces a non-perturbative spectrum out of perturbative diagrams, as we discuss next.

The presence of massive gluons in $CSQCD_S$ produces [21]-[23] triangle diagram anomalies in the effective vertices of reggeon diagrams. The contribution of the anomalies is (not surprisingly) strongly dependent on ultra-violet and infra-red cut-offs and so different “solutions” of the theory can be obtained, depending on how such cut-offs are handled. The essential part of our reggeon diagram analysis (described in Appendix C) is the initial imposition of a transverse momentum cut-off. This cut-off produces a violation of gauge invariance Ward identities for the anomaly vertices. As a result, infra-red transverse momentum divergences appear which, when the quarks involved are massless, produce residue amplitudes that contain “anomaly poles” resulting from infra-red chirality transitions. (An anomaly pole is produced, in part, by a pinching of massless particle and antiparticle poles in the same zero momentum propagator and so, automatically, involves a chirality transition.) The identification of anomaly poles as chiral Goldstone boson particle poles provides a crucial mechanism for a bound-state, confining and chiral symmetry breaking, spectrum (and the appropriate amplitudes) to appear via the contribution of anomalies and transverse momentum infra-red divergences.

Because our starting point is perturbative reggeon diagrams, the final amplitudes we obtain are not very far from perturbation theory. Very complicated multiparticle diagrams are involved and there is an elaborate phenomenon of cut-off dependent infra-red divergences coupled to triangle diagram anomalies. Nevertheless, both confinement and chiral symmetry breaking have a diagrammatic description. The primary reason that the physics involved stays perturbative is the existence of an infra-red fixed point due to the large number of quarks. By preventing the infra-red growth of α_s , the infra-red fixed point also produces infra-red scaling properties for reggeon interaction kernels that are vital for the emergence of physical scattering amplitudes via infra-red divergences.

Because both the infra-red fixed-point and infra-red effects of the chiral anomaly are crucial, it is essential that all quarks, including the sextet sector, are massless (initially). In this paper, we will discuss only how vector boson masses are generated by the sextet higgs mechanism. This mass generation is responsible for raising all effects of the sextet sector to momenta at or above the electroweak scale. This is necessary, of course, to obtain normal QCD at low energies since, within massless QCD_S , α_s remains less than it’s fixed point value ($\approx 1/34$). The familiar, larger, value of α_s is obtained only after an effective low-energy theory is obtained by integrating out the sextet sector. In addition, to be physically applicable, triplet quark effective masses must also be added to the S-Matrix of QCD_S . We will not discuss the origin of ef-

fective quark masses. This is related to the unification of QCD_S and the electroweak sector of the Standard Model in a larger theory[9] and we will discuss this in forthcoming papers[10]. Fortunately, for most of our discussion in this paper, only vector boson masses are relevant and so the issue can be avoided.

The transition from $CSQCD_S$ to QCD_S is to be achieved via supercritical RFT and the phase transition appearance of the Critical Pomeron[3]. If this can be carried through in full detail, the regge behavior of QCD_S , together with the infinite momentum hadron states, will be obtained from the much simpler infra-red divergence and anomaly structure that appears in $CSQCD_S$. In particular, within (infinite momentum) QCD_S , confinement and chiral symmetry breaking will be understood as resulting from dynamical infra-red chirality transitions produced by wee gluon interaction anomalies. However, as we already emphasized above, the spectrum of physical states will be significantly limited compared to that normally anticipated. Only states that correspond to Goldstone bosons in $CSQCD_S$ will be present. These states (and only these) have, as a consequence of the flavor anomaly, a wee gluon content that produces the infra-red divergent amplitudes giving the, eventual, physical amplitudes. Pions and nucleons are included amongst such states, but flavor singlet Goldstone bosons, unstable resonances and glueballs, are all excluded (as asymptotic states). As we have already emphasized, the absence of hybrid sextet/triplet baryons in QCD_S is crucial for the stability of the N_6 and, hence, for our explanation of the origin of dark matter.

In conventional QCD, the only non-conserved axial U(1) charge is that coupling to the short-distance topological anomaly. If this were the case in QCD_S , the U(1) symmetry (essentially the sextet symmetry) associated with the η_6 would be unbroken. In addition to being the analog of the usual higgs scalar, the η_6 would be a light axion of the kind that is ruled out experimentally. In our solution of QCD_S the anomaly vertices that are initially obtained by imposing a cut-off, and that are responsible for the dynamical “wee gluon” component of infinite momentum physical states, break both the sextet and triplet U(1) symmetries and so there is no light axion. Consequently, although the η_6 appears, at first, to be a Goldstone boson of the appropriate kind to appear as a physical state, there is a multigluon regge exchange (a daughter of the pomeron) that mixes with it. This mixing, presumably, generates a large (electroweak scale) mass for the η_6 . The η_6 also couples to the triplet sector via the gluon intermediate state and if it has an electroweak scale mass the mixing will be primarily with the $t\bar{t}$ state. Consequently, as we will briefly discuss, the η_6 could actually be responsible for top production at the Tevatron.

Clearly, that the infra-red anomaly contributions persist, via longitudinal wee gluons, after the removal of the large k_\perp cut-off and the restoration of SU(3) gauge symmetry, is a central element of our construction of QCD_S . It is well-known that the contribution of longitudinal wee gluons is an, a priori unresolved, ambiguity in the

infinite momentum quantization of QCD which is closely related to the well-known Gribov problem[24] and, therefore, to the choice of vacuum at finite momentum. In effect, therefore, we resolve this ambiguity in QCD_S by constructing the high-energy behavior via $CSQCD_S$.

It is well-known that both s -channel and t -channel unitarity (via reggeon unitarity) impose very strong constraints on the behavior of a theory in multi-regge limits. A solution of QCD in all such limits necessarily determines how unitarity, the physical spectrum, and the validity of perturbation theory all coexist. Obtaining such a solution is, therefore, likely to be almost as difficult as solving the full theory. As we have said, according to our arguments the multi-regge limits of QCD_S are described by the Critical Pomeron[3], which is known to satisfy all unitarity requirements. In addition, we are able to give a diagrammatic construction in which the connection between perturbation theory, the pomeron, and the physical bound state spectrum is clear. If everything goes through as we describe, it will be apparent that QCD_S is a version of QCD that, perhaps uniquely, satisfies all general requirements.

On the lattice, it would be very difficult, if not impossible, to introduce the co-ordinated infra-red dynamical fluctuations of longitudinal wee gluons and the Dirac sea that provide the anomaly couplings, and consequent infra-red divergences that lead to the infinite momentum QCD_S S-Matrix. Not surprisingly, perhaps, within the lattice framework, the infra-red fixed-point that we have discussed is generally believed[25] to be associated with a non-confining continuum theory and there is no sign of the confining “anomaly-driven” S-Matrix that we have discovered.

Similarly, there are general arguments[26] that the infra-red fixed-point in QCD_S will produce Green’s functions that are conformally invariant in the infra-red region and do not contain any particle-like physical states. In fact this is, essentially, the infra-red scaling property of reggeon kernels which plays a central role in our analysis. Clearly, it is a subtle challenge to find the asymptotic states and S-Matrix amplitudes that emerge from our construction. They do not appear within quark or gluon Green’s functions. Indeed, their existence depends crucially on S-Matrix fermion anomalies that also do not appear in off-shell Green’s functions. For the reasons that we elaborate on in Appendix C, it may be necessary to consider the (on-shell) scattering of vector bosons with left-handed couplings to quarks, to see the emergence of the desired amplitudes.

Section 2 is devoted to the high-energy solution of $CSQCD_S$. Our essential aim is to focus on the physics that underlies this solution. To this end, we keep the discussion at a fairly broad level and supplement it with Appendices. In Appendix A we describe the formal infra-red and ultra-violet β -function properties that are needed to connect $CSQCD_S$ to QCD_S . We do not use (in Section 2) the full multi-regge theory that is necessary to actually derive the solution that we describe. Instead, we use the anomaly-pole vertex method developed in [22]. Needed properties of the triangle

anomaly and the contribution of the anomaly pole are described in Appendix B. In Appendix C we outline our full multi-regge program and, as part of our description, we include (very briefly) the historical development which led to our association of the Critical Pomeron with QCD_S . Since many of the details of how the transition from $CSQCD_S$ to QCD_S is described by the Critical Pomeron have still to be worked out we give, in Section 3, only a brief outline of the features that are relevant for the purposes of this paper.

We begin the process of combining the electroweak sector with QCD_S in Section 4. In particular, we show how masses for the electroweak bosons are generated by anomaly interactions that result from the presence of wee gluons in infinite momentum physical states. This is the infinite momentum S-Matrix analog of vacuum generation of the masses. Most importantly, we see that the mass scale is determined by the coupling of wee gluons to sextet quarks. We can then carry the knowledge of this coupling over to the coupling of the pomeron to sextet quark states and, in particular, to multiple Z^0 and W^\pm states.

In Sections 5 and 6 we discuss processes that might be seen (or may have already been seen) at current accelerators and could provide evidence for the existence of the sextet sector. In Section 5 we discuss diffractive deep-inelastic scattering and suggest that the most dramatic large x and Q^2 event presented[27] by ZEUS, may have been diffractive production of a Z^0 . Sextet quark physics that might be seen at the Tevatron is the focus of Section 6. We describe a number of small cross-section effects that might be seen in diffractive, and diffractive related, processes involving W^\pm and Z^0 vector bosons. We also suggest that $t\bar{t}$ production could originate from the η_6 , even though this process can be understood perturbatively. The interpretation of the top quark mass would be different and non-perturbative decay modes should also be seen, at some level. A jet excess at large E_T would provide supporting evidence for this proposal since, in this case, α_s evolution should stop at $E_T \sim m_{top}$.

If the sextet sector exists, the LHC will most probably be the discovery machine. Sections 7 and 8 are devoted to explaining why we expect that dramatic effects will be seen. In Section 7 we discuss dark matter and the cosmic ray phenomena that tell us that the sextet sector could appear at the LHC. We discuss the specifics of what we expect to see at the LHC in Section 8. While jet cross-sections and cross-sections for multiple vector boson production will be orders of magnitude larger than expected, the double pomeron cross-section for electroweak vector boson pairs, which can be studied (in part) during the initial low luminosity running, may well be the most definitive early evidence that is seen. There could be spectacular events in which the forward protons are tagged and only large E_T leptons are seen in the central detector. “Dark matter”, in the form of sextet neutron/antineutron pairs, should have significant inclusive cross-sections and may even be produced in double pomeron exchange. If so, this would be really dramatic!

2. COLOR SUPERCONDUCTING QCD_S

2.1 Symmetry Breaking, Reggeization, and Infinite Momentum States

The breaking of the $SU(3)$ color symmetry of QCD_S to $SU(2)$ can be achieved with an asymptotically free, complex color triplet, scalar field. (This is discussed in more detail in Appendix A.) As a consequence of the symmetry breaking, $CSQCD_S$ contains an $SU(2)$ triplet of massless gluons, plus two $SU(2)$ doublets (with mass $\frac{2}{\sqrt{3}}M$) and one singlet (with mass M) of massive gluons. Each $SU(3)$ triplet quark gives one complex $SU(2)$ doublet and one singlet quark. Each $SU(3)$ sextet quark gives one complex $SU(2)$ triplet, one complex doublet, and one singlet quark. Reflecting the absence of any corresponding chiral symmetry in QCD_S , there is obviously no chiral symmetry relating the, sextet originating, $SU(2)$ complex triplet to either of the $SU(3)$ triplet originating representations.

All quarks and gluons (massive or not) are reggeized, but only the $SU(2)$ singlets have infra-red finite regge trajectory functions. The infra-red scaling behavior of various “transverse momentum kernels” that describe the interactions of reggeized quarks and gluons will be an essential ingredient of the following analysis. The scalar particle produced by the scalar field does not reggeize and so at the non-leading power level $CSQCD_S$ is, presumably, a non-unitary theory - implying that only the leading high-energy behavior of QCD_S can be constructed via $CSQCD_S$.

The status of the full program that we have developed to construct the multi-regge behavior of $CSQCD_S$ is outlined in Appendix C. We believe that this program, as it is now formulated, would give the high-energy behavior of QCD_S unambiguously if pursued to completion. However, we can arrive much more simply at the physics involved if we utilise the approach that we developed in [22]. In that paper, we introduced a procedure that was designed to bypass the multi-regge construction and instead obtain directly the $CSQCD_S$ scattering amplitudes for infinite momentum states. This procedure is what we now describe.

We note, before we start, that if high-energy states and amplitudes can be derived from perturbative reggeon diagrams, then the parton model must have a broad validity, well beyond leading-twist perturbation theory. For this to be the case, the “naive” validity of the perturbative vacuum at infinite momentum must hold for deeper reasons. This can be so if infinite momentum states have a universal “wee parton” component that carries the finite momentum “properties of the vacuum”. (Note that, although it is not directly relevant at this point, regge pole factorization properties for the pomeron are, most probably, a pre-requisite for a universal wee parton distribution in hadrons.) As we shall see, it is indeed a universal wee gluon

component of infinite momentum states that determines our solution of $CSQCD_S$.

2.2 Pion Anomaly Pole Vertices

The primary assumption in [22] was that the wee gluon properties of the physical states could be obtained[¶] from properties of the chiral anomaly and “anomaly pole” vertices. It is well-known that an anomaly pole appears, in particular kinematic circumstances, in a three-point vertex of local currents when the triangle diagram anomaly is present and when the fermions producing the anomaly are massless. When the vertex involves an axial current that is the generator of a chiral symmetry that is spontaneously-broken, this pole can be directly interpreted as a Goldstone boson particle pole associated with the symmetry breaking.

The invariant functions of a triangle diagram depend on the invariants k_1^2 , k_2^2 , and q^2 , where, as shown in Fig. 1(a), k_1, k_2 and q are the momenta entering at each of the vertices.

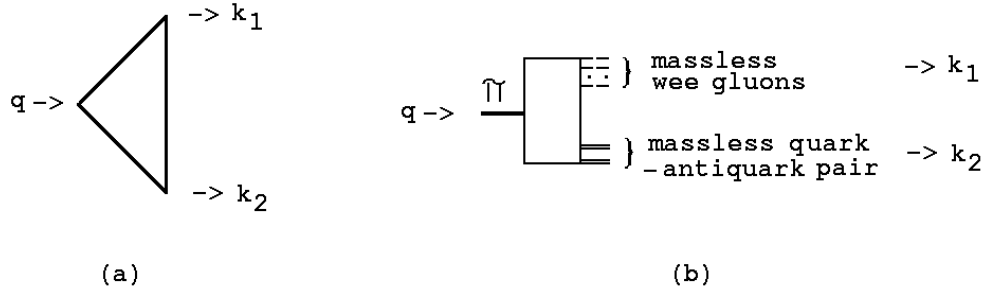


Fig. 1 (a) Triangle momenta (b) How wee gluons give a pion anomaly pole.

The pole is present when either

$$k_1^2 = k_2^2 = 0, \quad q^2 \rightarrow 0, \quad \text{or} \quad k_1 = 0, \quad k_2^2 = q^2 \rightarrow 0 \quad (2.1)$$

and the residue is determined by the anomaly. (Some details of how the pole is generated are given in Appendix B.)

We anticipate that the occurrence of anomaly poles in regge limit effective triangle diagrams will be a widespread phenomenon in the full multi-regge analysis of $CSQCD_S$. They appear whenever components of the relevant currents (not the full currents) appear as effective vertices in a triangle diagram. Poles associated with a flavor anomaly current component are Goldstone boson particle poles that are, in effect, dynamically generated. As illustrated in Fig. 1(b), the kinematics producing

[¶]We expect this to be an outcome of the full multi-regge program and we emphasized in [22] that if the assumptions made appeared to be ad-hoc this was, in large part, because of our deliberate efforts to avoid the full complexity of multi-regge theory.

a Goldstone (pion) pole can occur when a set of wee gluons produces a divergence at $k_1^2 = 0$ and couples via an effective triangle diagram to a quark-antiquark pair that carries a light-like momentum k_2 . In this Section, we will refer to all quark/antiquark (triplet or sextet) Goldstone bosons in $CSQCD_S$ as “pions” and, when we need to, will refer to quark/quark or antiquark/antiquark Goldstone bosons[28] as “nucleons”. Effectively, all of our discussion of pions will also apply to nucleons, even though we will not usually say so explicitly. Poles associated with the U(1) anomaly do not contribute as particle poles but instead contribute as δ -functions that conserve wee gluon transverse momenta during an interaction.

The underlying calculations needed to demonstrate the existence of the initial anomaly pole vertices we require can now be found in [21]. In calculations carried out after [22] was published, we showed explicitly how, in the scattering of electroweak vector bosons, effective vertices containing a triangle diagram are generated by the contraction of larger loop diagrams, in the channel with pion exchange quantum numbers. As a result, we can anticipate that in general scattering processes involving an infinite momentum vector boson, if a transverse momentum cut-off is imposed, a pion anomaly pole will indeed appear with the wee gluon couplings we assumed to exist. This should be sufficient to show that a massless on-shell pion carrying light-cone momentum k_+ has a coupling to wee gluons (carrying total light-cone momentum k_- , with $k_-/k_+ \rightarrow 0$) given by the anomaly pole residue of a triangle diagram that is generated as illustrated in Fig. 2. (The use of vector boson scattering states is explained in Appendix C.)

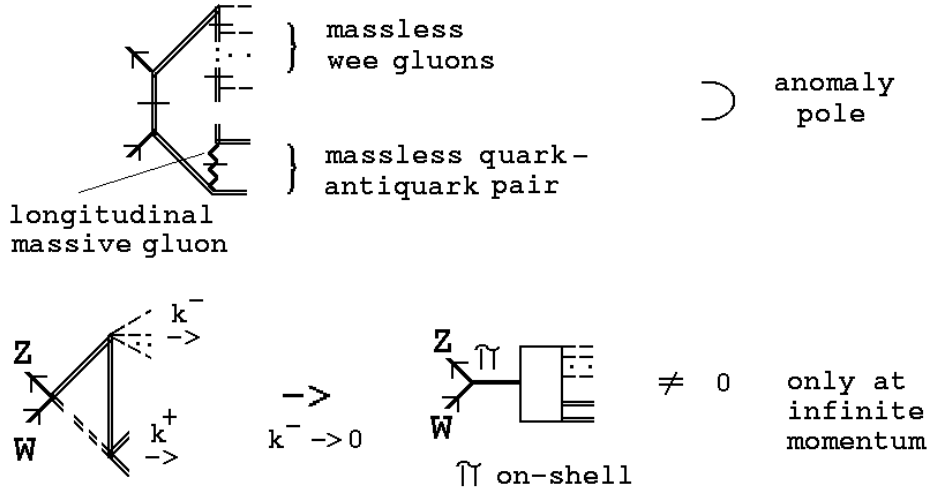


Fig. 2 Anomaly pole generation in an effective triangle diagram. (The hatched lines are on mass-shell.)

The coupling shown in Fig. 2 involves a massless quark-antiquark pair that has

a vector-like helicity and any number of “wee gluons”, that are also in a vector-like state. The dashed line in the triangle diagram is a zero momentum quark propagator that, as discussed in Appendix B, generates the anomaly pole and also produces a chirality transition. According to (B.17), in an “infinite momentum” frame reached via a boost $a_3(\zeta)$, the momentum dependence of the anomaly pole coupling is

$$[k_+ k_- \sinh \zeta] \quad (2.2)$$

which is finite when $k_- \rightarrow 0$, if $k_- \cosh \zeta$ is kept finite. It is important that (as we will discuss further later) it is the longitudinal component of the massive gluon that is responsible for the quark/antiquark vertex of the triangle diagram.

As we develop a complete dynamical picture in the following, we will introduce a variety of anomaly pole effective vertices whose existence is a natural extrapolation of existing vertices but, for which, the underlying (very complicated) multi-regge calculations still need to be performed.

2.3 Transverse Momentum Kernels and Infra-Red Divergences

In [22] we also argued that, because the anomaly pole is generated by a light-cone internal momentum region within the triangle diagram, we could use transverse momentum diagrams to discuss wee gluon interactions within the infinite momentum pion state. (Again, this should, straightforwardly, be the case in the multi-regge framework of Appendix C.) The coupling (2.2) is defined at $k_\perp = 0$, where k_\perp is the transverse momentum of the wee gluons. That it is non-zero is correlated with the fact that, for $k_\perp \neq 0$, the anomaly pole contribution to the effective triangle diagram violates the wee gluon Ward identity (for reasons discussed in Appendix B). A direct consequence is that infra-red divergences appear in the transverse momentum diagrams and dominate the physical pion scattering amplitude. (In the multi-regge framework, a transverse momentum cut-off is initially responsible for the failure of Ward identities that then leads to the occurrence of divergences and the correlated appearance of anomaly pole couplings.)

To describe the infra-red divergences that occur, we must first describe the infra-red properties of the transverse momentum kernels that are involved. These kernels are defined in more detail in Section IIIB of [22], where a detailed review of elastic scattering reggeon diagrams is also given. We begin with the kernels $K_N^I(\underline{k}, \underline{k}')$ that involve only the SU(2) triplet of massless gluons. (I denotes SU(2) color.) When the color of the multigluon state is non-zero, infra-red divergences give (in a sense explained in [22])

$$\mathcal{Q} \left\{ \begin{array}{c} \underline{k}_1 \text{---} \text{---} \text{---} \\ \text{---} \text{---} \text{---} \\ \underline{k}_N \text{---} \text{---} \end{array} \right\} \boxed{K_N^I} \left\{ \begin{array}{c} \text{---} \text{---} \text{---} \text{---} \underline{k}'_1 \\ \text{---} \text{---} \text{---} \\ \text{---} \text{---} \text{---} \text{---} \underline{k}'_N \end{array} \right\} = K_N^I(\underline{k}, \underline{k}') \rightarrow \infty, \quad Q^2, I \neq 0 \quad (2.3)$$

As a result, the sum of all gluon transverse momentum diagrams in any colored channel exponentiates to zero.

When $I = 0$ and $Q^2 \neq 0$, the kernels $K_N^0(\underline{k}, \underline{k}')$ are finite and have an important scaling property, as described in [22]. As a result, there is no exponentiation of divergences in color zero gluon channels. However, the disappearance of all colored multigluon states is not confinement since gluon poles remain in the color zero diagrams. Confinement is produced when the remaining $Q^2 = 0$ singularity in color zero channels is absorbed into a “condensate”, as we describe below.

The most important contribution of the K_N^0 kernels comes when a color zero set of massless gluons accompanies another SU(2) color zero transverse momentum state, as can be the case in states produced by the pion anomaly pole couplings. In Fig. 3 we show the kernel $K_R(\hat{k}, \underline{k}, \hat{k}', \underline{k}')$ describing the interactions of massless gluons with the massive (SU(2) singlet) reggeized gluon and the kernel $K_Q(\hat{k}, \underline{k}, \hat{k}', \underline{k}')$ describing the analogous interaction with an SU(2) singlet quark-antiquark pair.

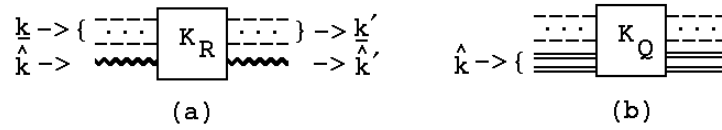


Fig. 3 Kernels for massless gluon interactions with (a) a massive reggeized gluon (b) a quark-antiquark pair.

Ward identities require that both K_R and K_Q vanish when either $\underline{k} \rightarrow 0$ with \underline{k}' fixed or when $\underline{k}' \rightarrow 0$ with \underline{k} fixed. But, because these kernels have a dimension of [momentum]² and additional non-zero mass and momentum scales (i.e. M^2 and \hat{k}^2) are present, we expect that these kernels neither vanish, nor have an infra-red scaling property, when $\underline{k} \sim \underline{k}' \rightarrow 0$. As a result, whenever the interactions of Fig. 3 exist, infra-red divergences again cause the sum of all diagrams to exponentiate to zero.

However, as illustrated in Fig. 4(a),

$$\begin{aligned}
 \tau = -1 \{ \text{diagram with } K_R \} &= \text{diagram with } K^0 \\
 \tau = -1 \{ \text{diagram with } K_Q \} &= \text{diagram with } K^0
 \end{aligned}
 \tag{a} \qquad \tag{b}$$

Fig. 4 Reggeon states without interaction kernels.

because of helicity conservation in the massless quark and gluon sector, there is no transverse momentum kernel describing the interaction of negative signature, color

zero, massless gluons with the massive reggeized gluon. This is because a multigluon state containing an odd number of gluons and carrying $SU(2)$ color zero necessarily has “anomalous color charge parity”, i.e. the color charge parity is necessarily positive and can not be equal to the negative signature. Similarly, as illustrated in Fig. 4(b), for a massless quark-antiquark state that carries negative signature, color zero, and normal color charge parity, there is also no interaction.

Related to the lack of interactions, transverse momentum states of the kind shown in Fig. 4 will couple only through anomalies. As a result, there will be no exponentiation of divergences in reggeon channels with these quantum numbers. Instead, the scaling property of the massless gluon kernels leads to an overall divergence.

2.4 Pion Scattering Amplitudes Via Infra-Red Divergences

In [22] we considered feynman diagram contributions to the particular transverse momentum diagram shown in Fig. 5, in which there are three wee gluons in each of the pion channels and also in the pomeron channel.

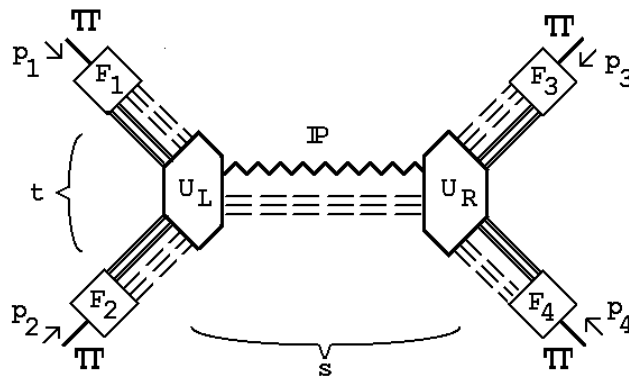


Fig. 5 A transverse momentum diagram for pion scattering.

(The notation in Fig. 5 is the same as for Fig. 2.) Because of the foregoing discussion, this diagram is amongst the simplest, describing pion scattering, that contain a transverse momentum divergence that does not exponentiate to zero. In [22] we carried out a detailed infra-red analysis to extract the resulting amplitude.

We will not reproduce the analysis of [22] here but, rather, will elaborate on features of the underlying physics that we did not discuss in [22]. For this purpose we need to describe, briefly, the kinematics involved in the analysis. The kinematics were chosen so that each of the initial and final state pions was in an infinite momentum frame, reached by an appropriate boost, such that an anomaly pole residue corresponding to (2.2) could give the contribution of each of the four external pion couplings F_i . To also produce internal triple-regge anomaly interactions, the wee gluons in the outgoing pions were associated with light-cones whose space direction is

orthogonal to that of the incoming wee gluon light-cones. We, therefore, introduced distinct Lorentz frames as follows. We calculated the left-hand part of Fig. 5 in a “left-hand finite momentum frame” in which p_1 and p_2 have the form^{||}

$$\begin{aligned} p_1 &= k^{1+} + q^{1-} = k_{1-} + q_{1+} \\ &= \left(\frac{k}{\sqrt{2}}, \frac{k}{\sqrt{2}}, 0, 0\right) + \left(\frac{q}{\sqrt{2}}, -\frac{q}{\sqrt{2}}, 0, 0\right) \end{aligned} \quad (2.4)$$

$$\begin{aligned} p_2 &= -k^{2+} - q^{2-} = -k_{2-} - q_{2+} \\ &= -\left(\frac{k}{\sqrt{2}}, 0, \frac{k}{\sqrt{2}}, 0\right) - \left(\frac{q}{\sqrt{2}}, 0, -\frac{q}{\sqrt{2}}, 0\right) \end{aligned} \quad (2.5)$$

where q^{1-} and q^{2-} are, respectively, the wee gluon momenta in F_1 and F_2 . For simplicity, we took the scale of the light-cone momenta for all on-shell pions to be k and the scale of all wee gluon (longitudinal) momenta to be q although, as we discuss further below, this is clearly not essential. Since

$$p_1^2 = p_2^2 = 2kq \quad (2.6)$$

q is both the wee gluon scale and the scale which puts pions on-shell as it vanishes.

The right-hand part of Fig. 5 was calculated in a “right-hand finite momentum frame” in which

$$\begin{aligned} p_3 &= k^{2+} + q^{2-} \\ &= \left(\frac{k}{\sqrt{2}}, 0, \frac{k}{\sqrt{2}}, 0\right) + \left(\frac{q}{\sqrt{2}}, 0, \frac{-q}{\sqrt{2}}, 0\right) \end{aligned} \quad (2.7)$$

$$\begin{aligned} p_4 &= -k^{1+} - q^{1-} \\ &= -\left(\frac{k}{\sqrt{2}}, \frac{k}{\sqrt{2}}, 0, 0\right) - \left(\frac{q}{\sqrt{2}}, -\frac{q}{\sqrt{2}}, 0, 0\right) \end{aligned} \quad (2.8)$$

and so we also have

$$p_3^2 = p_4^2 = 2kq \quad (2.9)$$

The full scattering amplitude for Fig. 5 was calculated in the “infinite momen-

^{||}The notation is straightforward in that k^{1+} is a vector with raised index component along the light-cone defined by the positive $\{1\}$ - axis (and all other othogonal components are zero). Similarly q^{1-} is a vector with raised index component along the light-cone defined by the negative $\{1\}$ - axis. The same vectors can be labeled via lowered index components as usual.

tum frame” in which

$$\begin{aligned}
p_1 &= \left(C \frac{k+q}{\sqrt{2}}, \frac{k-q}{\sqrt{2}}, 0, S \frac{k+q}{\sqrt{2}} \right) \\
p_2 &= - \left(C \frac{k+q}{\sqrt{2}}, 0, \frac{k-q}{\sqrt{2}}, S \frac{k+q}{\sqrt{2}} \right) \\
p_3 &= \left(C \frac{k+q}{\sqrt{2}}, 0, \frac{k-q}{\sqrt{2}}, -S \frac{k+q}{\sqrt{2}} \right) \\
p_4 &= - \left(C \frac{k+q}{\sqrt{2}}, \frac{k-q}{\sqrt{2}}, 0, -S \frac{k+q}{\sqrt{2}} \right)
\end{aligned} \tag{2.10}$$

where $C = \cosh \zeta$, $S = \sinh \zeta$, and so

$$\begin{aligned}
s &= (p_1 + p_3)^2 \xrightarrow{q \rightarrow 0} (C^2 + S^2)k^2 \sim 2C^2k^2 \quad C \rightarrow \infty \\
t &= (p_1 + p_2)^2 \xrightarrow{q \rightarrow 0} -k^2
\end{aligned} \tag{2.11}$$

We combined the mass-shell limit $q \rightarrow 0$ and the regge limit $s/t \rightarrow \infty$ by taking

$$q \sim 1/C \rightarrow 0 \tag{2.12}$$

Note that, as is apparent from (2.10), the wee gluon momentum q is exchanged only as a zero transverse momentum contribution in the infinite momentum frame.

The internal couplings U_L and U_R appearing in Fig. 5 are anomaly pole contributions from effective vertices of the form shown in Fig. 6

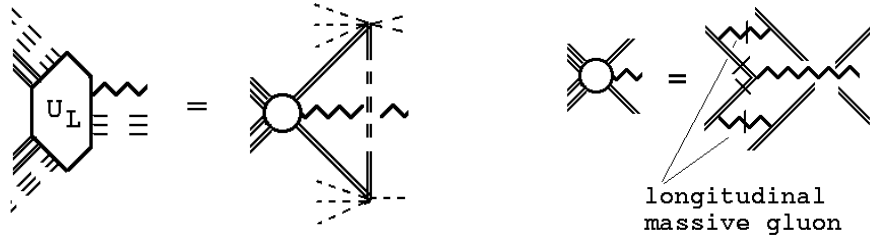


Fig. 6 An anomaly pole coupling.

(These vertices are illustrated in more detail in Fig. C6). Because the anomaly poles are integrated over, they contribute as “anomaly δ -functions” that produce a separate conservation of transverse momentum for the massless gluon interactions. This separate momentum conservation allows these interactions to be factorized off

from the remaining “hard interaction”. As a result, the diagram of Fig. 5 has an overall logarithmic divergence from the region where the transverse momenta of all massless gluons are scaled uniformly to zero. After this divergence is factorized off (as a zero transverse momentum “reggeon condensate”) and the pion poles in each channel are also extracted, the amplitude obtained has the form

$$\begin{aligned}
A_{\pi\pi\pi\pi} &\sim \prod_i \{F_i \text{ anomaly pole coupling}\} \{\text{quark } k_{i\perp} \text{ integrals}\} \\
&\times \prod_{j=L,R} \{U_j \text{ anomaly amplitude}\} \{\text{massive gluon propagator}\} \\
&\sim \left\{ \frac{k C q}{M^2} \right\}^4 \left\{ \frac{(kC)}{M^2} \frac{(kCq)}{M^2} \right\}^2 \left\{ C q \right\}^4 \left\{ \frac{1}{t + M^2} \right\}
\end{aligned} \tag{2.13}$$

Writing $t \sim k^2$ and $s \sim C^2 k^2$, (2.13) can be rearranged to give

$$A_{\pi\pi\pi\pi} \sim \left[\frac{C q}{M} \right]^8 \left[\frac{s q^2}{M^4} \right] \left[\frac{t}{M^2} \right]^2 \left[\frac{s}{t + M^2} \right] \tag{2.14}$$

Since the first two square brackets in (2.14) are finite constants when the limit (2.12) is taken, the kinematic structure of the pion scattering amplitude we obtain is, essentially, that of massive gluon exchange, i.e.

$$A_{\pi\pi\pi\pi}(s, t) = \left[\frac{t}{M^2} \right]^2 \left[\frac{s}{t + M^2} \right] \tag{2.15}$$

(Note that this result is obtained for $t \gg M^2$.) In higher-orders the massive gluon will reggeize, with an infra-red finite trajectory $\alpha_g(t)$ that satisfies $\alpha_g(M^2) = 1$. But, since the exchange of four reggeized gluons is involved, as we add all diagrams and go to higher-orders, only the even signature amplitude will survive. As a result, reggeization of the massive gluon will give

$$\left[\frac{s}{t + M^2} \right] \rightarrow \left[\frac{s^{\alpha_g(t)} + (-s)^{\alpha_g(t)}}{t + M^2} \right] \tag{2.16}$$

That is, reggeized gluon exchange will provide the leading contribution to the pomeron but there will be no gluon pole at $-t = M^2$.

2.5 Momentum Flows and Wee Gluon Couplings

The general dynamical structure of the diagrammatic contributions to $A_{\pi\pi\pi\pi}$ is illustrated in Fig. 7. Where there is a broken quark line (and a T) there is a chirality transition of a zero momentum massless quark. Wee gluon couplings, that we will discuss shortly, are denoted by a circle containing a w .

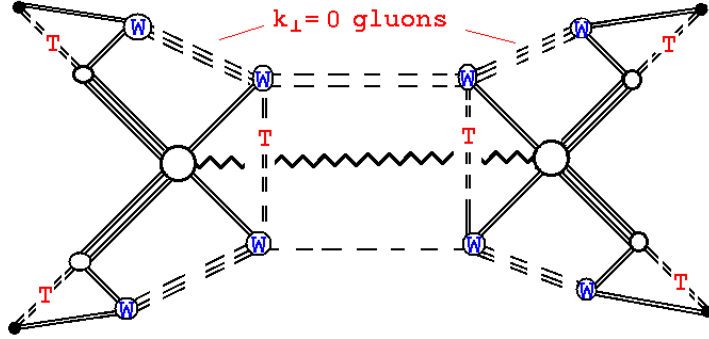


Fig. 7 Dynamical structure of the scattering amplitude.

Using the origin of the anomaly pole described in Appendix B, the scattering process can be interpreted as follows. A “pion” is created by the product of a physical quark field and a zero momentum “unphysical” antiquark field in which the Dirac sea is shifted. The antiquark becomes physical, via a chirality transition, that introduces an accompanying “semiclassical” anomalous wee gluon field (condensate) that effectively moves the sea back to its perturbative location. In the scattering process, the wee gluon field of an incoming pion is transformed into that of the outgoing pion by an anomaly coupling that involves a further rearrangement of the Dirac sea. The final state pions are created via a final shift of the Dirac sea that absorbs the anomalous wee gluon field.

The flow of large momentum ($\sim k$ in the finite momentum frame) through the left side of Fig. 7 is shown in Fig. 8(a),

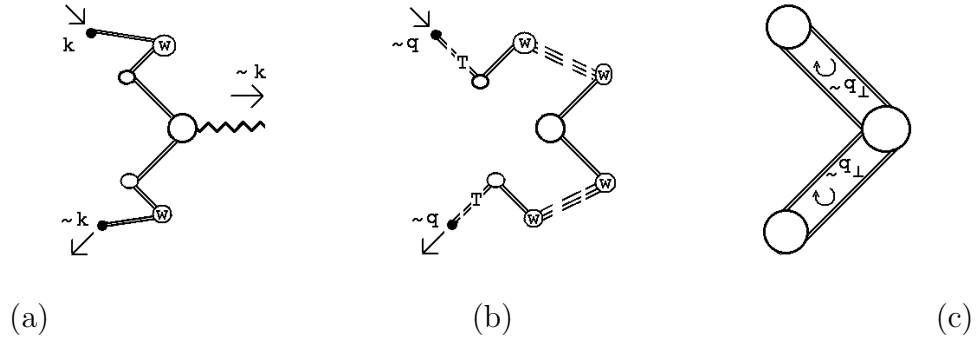


Fig. 8 Momentum flows.

while the flow of wee gluon longitudinal momentum ($\sim Cq$ in the infinite momentum frame) is, as shown in Fig. 8(b), along an (almost) orthogonal set of lines. Note that the large momentum flows along either the quark or the antiquark, but not both. The remaining momentum scale is the relative transverse momentum ($\sim q_\perp$) of the quark-antiquark pair which simply flows around a loop, as illustrated in Fig. 8(c). In

the finite momentum frame (“inside the pion”) the wee gluon limit $q \rightarrow 0$ gives the zero momentum required for the first and last chirality transitions. In the infinite momentum frame Cq provides the light-cone momentum flowing around the triangle diagram giving the anomaly δ -function. The “zero momentum” line in the δ -function triangle therefore has momenta much smaller than q in the finite momentum frame.

There are eight wee gluon couplings that originate from the chirality transitions. As we already noted, they are denoted by a circle containing a w in Fig. 7. A factor of Cq for each wee gluon coupling gives the factor of $[Cq/M]^8$ in (2.14). The other two factors in (2.14), apart from (2.16), arise from the integrations over the quark-antiquark relative transverse momenta. All of the factors in (2.14), apart from (2.16), are scaled by the vector boson mass M . The overall factor of M^{-16} can be traced back to the eight contributions of longitudinal massive gluon exchange. Four appear via anomaly pole vertices of the form appearing in Fig. 2, and are represented by small circles in Fig. 7. The other four appear in the two vertices, of the form shown in Fig. 6, represented by large circles in Fig. 7. In each case the longitudinal contribution of the on-shell massive gluon gives a contribution of the form

$$\text{“ } \frac{k_\mu k_\nu}{M^2} \text{ ”} \leftrightarrow [\text{wee gluon momentum}/M]_\mu [\text{quark transverse momentum}/M]_\nu \quad (2.17)$$

The existence of the amplitude (2.13) depends entirely on this interaction which, it is important to note, couples wee gluon related chirality transitions and small transverse momentum quark dynamics. Also, the appearance of a wee gluon momentum scale in the amplitude is crucially dependent on the presence of such transitions.

Clearly we need not have taken the wee gluon momentum scales of both scattering pions to be equal. In general the factor of $[Cq/M]^8$ in (2.14) would be replaced by a separate factor of $[(Cq)^2/M^2]^2$ for each scattering pion. Furthermore, we anticipate that if we were to carry through the complete multi-regge calculation of Appendix C, the wee gluon factor for each pion would be replaced by the (integrated) contribution of a wee gluon distribution $w(Cq/M)$ so that, in the pion amplitude,

$$\left[\frac{Cq}{M}\right]^8 \rightarrow \prod_{i=1,2} \left[\int d(Cq_i/M) (Cq_i/M) w(Cq_i/M) \right]^2 \equiv \left[\frac{C}{M}\right]^8 \prod_{i=1,2} \left[\int dq_i q_i w(q_i) \right]^2 \quad (2.18)$$

2.6 Higher-Order Diagrams

Consider now the higher-order diagrams that will add to that of Fig. 5. As we noted above, and discuss in more detail in [22], adding interactions amongst the wee gluons will not change the nature of the overall divergence. Similarly there will be no

change if the three wee gluons in the pomeron, and in each pion channel, are replaced by infinite sums over arbitrary (allowably different in each channel), odd, numbers of massless gluons that similarly have zero transverse momentum, carry overall SU(2) color zero, and have (anomalous) positive color charge parity. Again such wee gluons will have self-interactions but will not interact with the quark/antiquark pairs in the pions, or the SU(2) singlet reggeized, massive, gluon in the pomeron. The same discussion would also apply if the single massive gluon is replaced by any number of massive gluons (giving multiple pomeron exchange).

2.7 Pomeron Production Vertices

In the remainder of this Section, and the following Sections, we will go far beyond the explicit calculations of [21] and [22]. We will introduce effective vertices for which the underlying (in general, multi-regge) calculations have not, as yet, been carried out but whose existence is a natural extrapolation of the vertices that we have already discussed. We begin by considering, briefly, a set of effective vertices which are responsible for the vacuum production of pomerons that is one of the defining features of supercritical RFT.

A priori, it might appear that the anomaly δ function vertex of Fig. 6 could give rise to simple “vacuum production” of massive reggeized gluon pairs by wee gluons, as illustrated in Fig. 9(a).

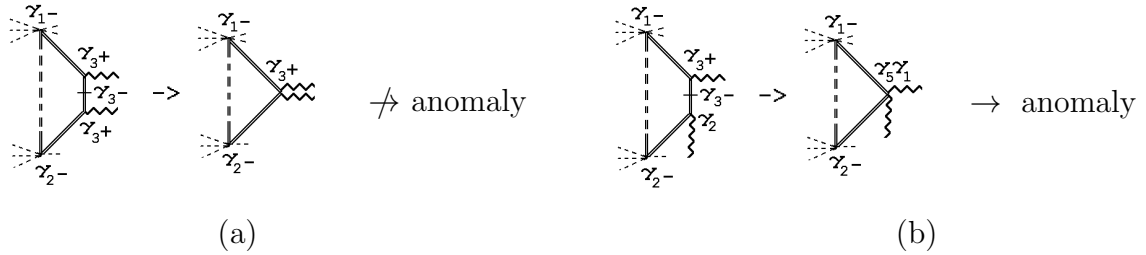


Fig. 9 Wee gluon vertices (a) that do not give an anomaly (b) that give an anomaly.

In fact, to have the axial vector structure for the anomaly, both gluons can not have the polarization needed to be exchanged in the scattering process. Instead, as illustrated in Fig. 9(b) one gluon must have a different polarization. Since the interaction can, nevertheless, take place some distance across the rapidity axis it leads to particle pole interactions within pomeron vertices.

The most general pomeron vacuum production vertices are generated as illustrated in Fig. 10. When these vertices are included, we reproduce the complete range of pomeron vertices that arise from the “vacuum production of pomerons” due to the pomeron condensate in the supercritical pomeron phase[29]. A more detailed study is needed to determine that the non-exchanged massive gluon in Figs. 9 and 10 is longitudinal.

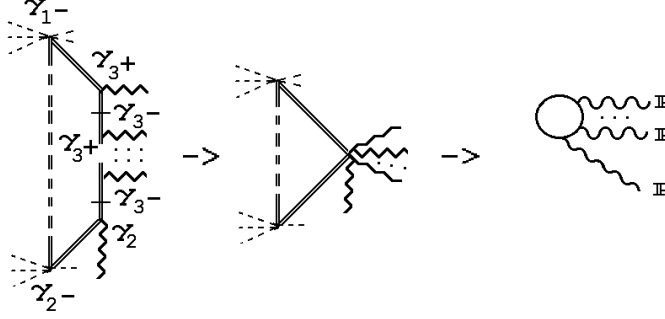


Fig. 10 Generation of pomeron vacuum vertices.

2.8 The Complete Set of Amplitudes and States

While it remains to be shown that the high-energy behavior of $CSQCD_S$ maps completely on to supercritical RFT, we will assume, in this paper, that the connection is established. Our major purpose, here, has been to elaborate the physics that is involved. As we have seen, the essential physics of $CSQCD_S$ is that a wee gluon condensate is produced by chirality transitions that are part of anomaly interactions introduced by the massive vector mesons. We can view the condensate as originating from a shift of the Dirac sea that produces states, and an S-Matrix, in which $SU(2)$ color confinement and chiral symmetry breaking completely determine the spectrum. The wee gluon condensate has no connection with instantons. It is a “semi-classical” infra-red effect that, as we discuss in the next Section, becomes a dynamical effect in QCD_S . Note also that, since the anomalous wee gluons in a pion can not be produced from the perturbative quark/antiquark component by normal perturbative interactions (without an anomaly-related chirality transition), we can say that there is no simple quark/antiquark component in the infinite momentum pion “wave function”.

We expect the complete set of (infinite momentum) physical scattering amplitudes in $CSQCD_S$ to be produced via a logarithmic divergence, as in our discussion of the amplitude obtained from Fig. 5. If this is the case, then any physical amplitude must involve initial and final scattering states that contain anomalous wee gluons. If such gluons appear only via anomaly pole vertices then, according to our discussion, all physical states must be color zero Goldstone bosons. Unfortunately, we have only been able to study on-shell pion amplitudes. If we were to carry through the multi-regge program of Appendix C, then we would obtain amplitudes for off mass-shell reggeized pions to scatter. This would give us much more information about how a pion appears as an anomaly pole and would, perhaps, allow us to determine the role played by chiral symmetry in ensuring that such a pole is present. For the present we assume that an anomaly pole occurs if and only if there is a chiral symmetry that can be broken spontaneously. We also assume that the anomaly pole mechanism provides the only possibility for the dynamical formation of bound state Goldstone bosons.

We can refer to the Goldstone bosons as created by a product of quark/antiquark operators alone provided we remember that the wee gluon component can be eliminated only by a shift of the Dirac sea in one of the operators. If we denote SU(3) color triplet quarks, generically, by q and SU(3) color sextet quarks, generically, by Q , the Goldstone boson states of $CSQCD_S$ obviously include all flavor non-neutral $q\bar{q}$ and $Q\bar{Q}$ pseudoscalar mesons. (There will be two separate $Q\bar{Q}$ states formed from SU(2) color triplets and doublets.) In Section 5, we will discuss how the flavor neutral mesons (the η_6 and the η_3) mix with pure gluon states and, hence, do not appear as Goldstone bosons. Because of the equivalence of quark and antiquark representations when the gauge symmetry is SU(2), there are also qq , $\bar{q}\bar{q}$, QQ , and $\bar{Q}\bar{Q}$ states that are Goldstone boson mesons in $CSQCD_S$ but will become baryons, by acquiring an additional quark (or antiquark) in QCD_S . Such states reflect real chiral symmetries[28] of $CSQCD_S$. (Again, the QQ states will appear as separate states formed from SU(2) color triplets and doublets.)

We will not discuss the dynamics of baryon formation in this paper, although we will briefly discuss the spectrum in the next Section. To discuss dynamics we need to know the full role of the SU(2) singlet quarks and gluons in $CSQCD_S$. According to the above argument, since they are not Goldstone bosons, they can not be physical states. If they are, nevertheless, “physical”, it must be that they appear as regge exchanges, without producing physical states. For example, within $CSQCD_S$ there can be a regge exchange involving the combination of a Goldstone boson “nucleon” and an SU(2) reggeized quark that can become a normal, reggeized, nucleon in $CSQCD$, as SU(3) color is restored.

2.9 Background Wee Gluon Interactions

A more subtle question is the role played by the SU(2) singlet gluon. In particular, is there an odd-signature amplitude involving only exchange of the SU(2) singlet gluon reggeon? A divergent amplitude can be produced by background wee gluon anomaly interactions, as illustrated in Fig. 11.

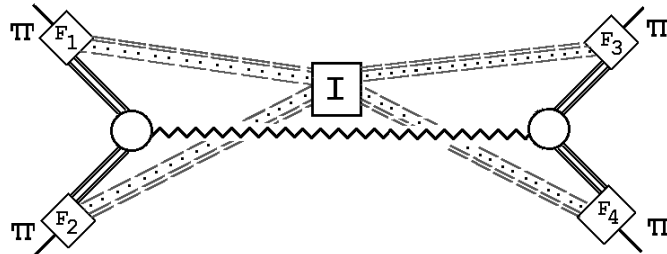


Fig. 11 Background Wee Gluon Interactions Accompanying Reggeon Exchange

In general, we would expect that there should be (multiple) chirality violating inter-

actions that involve just wee gluons, accompanying all interactions and contributing to the overall divergence. As we will see in Section 5, the existence of wee gluon interactions of this kind is essential for adding the electroweak sector of the Standard Model to $CSQCD_S$. Unfortunately, to establish the existence and nature of such interactions requires elaborate multi-regge calculations that have yet to be carried out. The interaction of Fig. 11 must contain anomaly effective vertices generated by the orthogonality of the γ -matrices involved, as illustrated in Fig. 12.

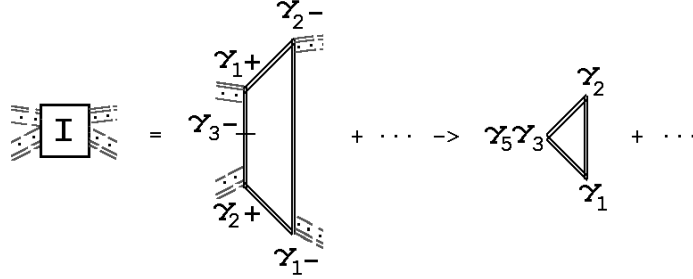


Fig. 12 A Background Effective Vertex Containing an Anomaly

If there is no anomaly, there will be an exponentiation of the divergences via even signature (BFKL) gluon interactions with the reggeon, as illustrated in Fig. 13, that will produce a zero amplitude. The anomaly vertex of Fig. 12 necessarily couples directly to the wee gluons in the scattering state, and so avoids the exponentiation.

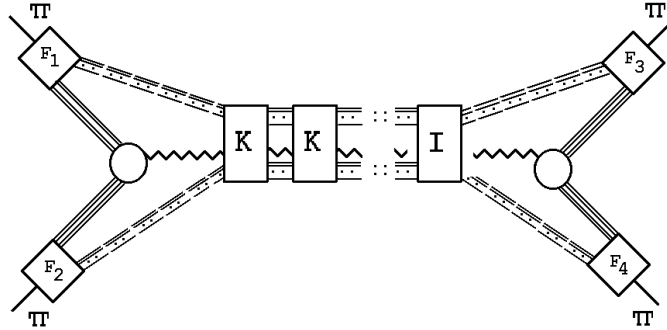


Fig. 13 Potential Exponentiation of the Wee Gluon Interaction

As $SU(3)$ symmetry is restored, the background wee gluon interaction should become $SU(3)$ symmetric. As a result, the non-zero $SU(3)$ color of the reggeon in Fig. 11 should lead to the vanishing of this amplitude. However, when the reggeon is replaced by an electroweak vector boson which does not carry color, as we discuss in Section 5, the corresponding amplitude will not vanish.

3. THE CRITICAL POMERON IN QCD_S

If the high-energy behavior of $CSQCD_S$ is mapped onto supercritical RFT, as discussed in the last Section (and in Appendix C), $SU(3)$ color will be restored via the Critical Pomeron phase transition. As part of this transition, the $SU(2)$ singlet gluon will become massless and decouple. Simultaneously, the wee gluon condensate will disappear and a corresponding dynamical degree of freedom will appear. That is, the shifting of the Dirac sea will become dynamical. Dynamical, gauge-invariant, infinite number), wee gluon combinations carrying octet color, will produce the chirality transitions illustrated in Fig. 7 (and many more). For this to happen, the longitudinal vector meson interactions, which at first sight should decouple as the color symmetry breaking is removed, must still be present - at zero light-cone momentum.

In fact, the role of zero light-cone momentum, longitudinal, gluons is a major ambiguity of light-cone quantization[30]. When we discuss wee gluons in a pion, as we did in the previous Section, we are essentially invoking light-cone quantization in a frame in which the pion carries light-cone momentum k_+ . For the dynamical wee gluon processes that we are discussing to be present the longitudinal, zero light-cone momentum, gluons must provide the interactions, of the form of (2.17), that are responsible for the occurrence of the chirality transitions (and anomaly poles) in Fig. 7. There is, of course, no vector gluon mass “ M ” in QCD_S . Consequently, there must be an intrinsic momentum scale μ that is generated as part of the symmetry restoration process that will provide the scale for dynamical wee gluon contributions in a hadron. Whether, or not, this scale should simply be identified with the normal dynamical scale of QCD_S remains to be determined. In any case, by constructing the high-energy behavior of QCD_S via $CSQCD_S$ we are, effectively, fixing the ambiguity of the role of zero light-cone momentum, longitudinal gluons.

The dynamical shifting of the Dirac sea produced by wee gluon interactions will, as we said above, no longer correspond to the introduction of a semi-classical gauge field, or condensate, in a fixed direction of the $SU(3)$ color group. Rather, the chirality transitions, which will be many in any scattering process, will correspond to random gauge field fluctuations within the color group. The transition from a fixed “magnetization” for the gauge field associated with Dirac sea shifts to a randomized, fluctuating, field, characterizes the nature of the “critical phenomenon” that is associated with the high-energy behavior of QCD_S . The shifting of the Dirac sea is the “order parameter” of the transition. In the supercritical phase this degree of freedom is ordered into a single, semi-classical, wee gluon gauge field contribution, while in the sub-critical phase it is random.

It is obviously essential for the quarks to be massless if the physics of the Crit-

ical Pomeron is to be as we have just described it. The chirality transitions can take place in a “perturbative manner” (i.e. within effective vertex triangle diagrams) only if the quarks are massless. We would expect, however, that the high-energy behavior is independent of the physical states acquiring masses and therefore would expect that the Critical Pomeron remains, at high-energy, even when effective quark masses are added to QCD_S . To add such masses and preserve the physics involved would appear, nevertheless, to be non-trivial. It would appear that the Dirac sea would have to undergo major shifts (as envisaged by Gribov[31]) in a random dynamical manner, as part of any scattering process and as part of the creation of asymptotic states. In fact, it now seems likely that the solution to this obviously complex problem is provided by the embedding of QCD_S and the electroweak sector of the Standard Model in “very special” unified theory[9, 10]. This unified theory should also answer the question of how the short-distance electroweak anomaly due to the sextet quarks is canceled.

The large transverse momentum (“short distance”) pomeron will be the least sensitive to the wee gluon phase transition. At large transverse momentum, therefore, the QCD_S pomeron will be approximately a short-distance (gauge-invariant) reggeized gluon combined with a color compensating dynamical, anomalous, wee gluon contribution. Also, at large transverse momentum, both triplet and sextet pions will have a wee gluon component that is the same as the pomeron, but with a short-distance quark-antiquark pair replacing the reggeized gluon. It can be shown that the quark-antiquark state in a pion reggeizes and so becomes gauge-invariant, like the reggeized gluon in the pomeron, but we will not discuss it in this paper. (Note that we expect that at large transverse momentum the quark and antiquark in a reggeized pion have equal dynamical status while, in an on-shell pion one or the other carries, essentially, all of the corresponding light-like momentum.)

As we said in the last Section, we also will not attempt to follow the formation of baryons as $SU(3)$ color is restored. However, there is one very important feature of baryon formation which is clear. Namely, there are no “hybrid states” formed, for example, by a sextet quark Q combining with a $\bar{q}\bar{q}$ triplet state that is a “nucleon” in $CSQCD_S$. This combination is possible in principle, but the Goldstone boson nucleon will have the wrong symmetry properties to combine with the $SU(2)$ singlet component of a sextet quark. In addition, for the complete $SU(3)$ invariant state to be formed it would be necessary to also have a $\bar{q}Q$ state in $CSQCD_S$ combining with an $SU(2)$ singlet \bar{q} (as the symmetry is restored) and, as is clear from the previous Section, this is prevented by the complex $SU(2)$ triplet component of the Q . We conclude, therefore, that the only new baryon states formed by the sextet sector are the sextet proton - the P_6 , and the sextet neutron - the N_6 . The importance of this conclusion will become apparent in later Sections.

We can enumerate the formation of the asymptotic states of QCD_S from those

of $CSQCD_S$, as follows.

1. “pions” $\leftrightarrow \{q\bar{q} + \text{wee gluons}\} \rightarrow \text{normal meson spectrum in } QCD_S$
2. “Pions” $\leftrightarrow \{Q\bar{Q} + \text{wee gluons}\} \rightarrow \Pi^\pm, \Pi^0, \text{ in } QCD_S$
3. “nucleons” $\leftrightarrow \{qq / \bar{q}\bar{q} + \text{wee gluons}\} + \{q / \bar{q}\}, \rightarrow \text{SU}(3) \text{ color singlet}$
 $\rightarrow \text{normal nucleon spectrum in } QCD_S$
4. “Nucleons” $\leftrightarrow \{QQ / \bar{Q}\bar{Q} + \text{wee gluons}\} + \{Q / \bar{Q}\}, \rightarrow N_6, P_6^\pm \text{ in } QCD_S$

In Section 5 we will discuss hard diffractive interactions of the pomeron with either a photon or an electroweak vector boson. In these interactions the wee gluon component has only a limited role and, most importantly, there are no wee gluon interactions. In these circumstances, we can continue to represent the wee gluon component as a zero transverse momentum “condensate”. Even though, in reality, it is a much more complicated dynamical contribution of wee gluons over a range of infra-red transverse momenta. As we will see, the effective vertices involved will not contain a longitudinal vector interaction and so, as a consequence, the scale of wee gluon couplings will be an important effect. It will be crucial that, as we determine from the electroweak mass scale in the next Section, the wee gluon couplings for triplet and sextet quarks are very different. This will be represented by distinct condensate couplings for triplets and sextets.

With the wee gluons treated as semi-classical, we will be able to use the anomaly pole mechanism to obtain a limited understanding of the production of sextet pions and the resultant production of W ’s and Z ’s in hard diffractive processes. Not surprisingly, the minimal representation of the dynamics of the wee gluon component will have major limitations. Most significantly, we will be able to apply the “condensate anomaly mechanism” only at large k_\perp and then, directly, only to the production of an “on-shell” sextet pion carrying light-like momentum. Dynamical wee gluons can, presumably, produce sextet pions at both small k_\perp and off-shell, but we will not try to discuss this explicitly. Instead, we first use the kinematic form given directly by the anomaly amplitude to go “off-shell”. This leads to rough order-of-magnitude estimates and (some) qualitative kinematic features of hard diffractive phenomena. We can then combine the knowledge of hard diffraction that we obtain, with regge theory, to discuss expectations for soft diffraction. We will argue that, at the LHC, the most immediate place to see that new physics is in evidence is likely to be the double pomeron exchange cross-section!

4. ELECTROWEAK VECTOR BOSONS AND THE SEXTET QCD SCALE

We consider, now, the addition of the electroweak vector boson sector to QCD_S . We first add a triplet $\{W^\pm, W^0\}$ of massless SU(2) gauge bosons with Standard Model left-handed couplings (with coupling constant g_w) to both triplet and sextet quarks. Later we will add a massless hypercharge gauge field Y (with coupling constant g_y) that also has Standard Model couplings to all quarks. We define “Standard Model” couplings for sextet quarks by recognizing that sextet antiquarks have the same SU(3) triality as triplet quarks. It is natural, therefore, for sextet antiquarks (quarks) to have the same electroweak couplings as triplet quarks (antiquarks). In fact, this is also what occurs when both kinds of quarks originate from an underlying unified theory[9]. In massless QCD_S there will be three flavor doublets of color triplet quarks that each produce a triplet of “pions” that have the quantum numbers to couple directly to the W ’s. The triplet of Pions produced by the single sextet doublet similarly has the quantum numbers to couple directly to the W ’s. We begin in $CSQCD_S$, however, because this will enable us to understand the generation of a vector boson mass in terms of anomaly pole pions and Pions. We will see how the wee gluon component of a scattering, infinite momentum, pion generates a mass for an exchanged vector boson, as we would expect if the universal wee gluon component of infinite momentum states is able to reproduce vacuum properties.

4.1 Background Wee Gluon Interactions

To obtain an infra-red divergent scattering amplitude involving W exchange, there must be a wee gluon exchange accompanying (but not interacting with) the W , as illustrated in Fig. 14.

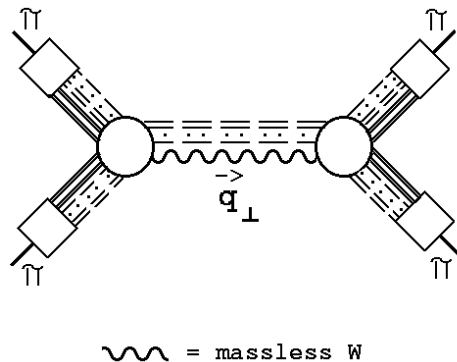


Fig. 14 Scattering via W exchange.

(Apart from the exchanged vector boson, the notation is the same as in Section 2.) However, because of the left-handed coupling, there will be interaction kernels, analogous to that of Fig. 3, for the W to interact with multi-gluon states that carry both normal and anomalous color charge parity. As a consequence, all infra-red divergent amplitudes will be exponentiated to zero, except for those produced by background wee gluons. Although the underlying multi-regge calculations remain to be carried out, we expect that there will be amplitudes analogous to that of Fig. 11, but with the gluon reggeon replaced by a (reggeized) vector boson. In this case, we expect that the full anomaly vertices, of the kind illustrated in Fig. 12, will not survive the exponentiation analogous to Fig. 13. Instead, the left-handed component of the axial-vector coupling shown in Fig. 12 will, because of the left-handed W coupling, contribute to an exponentiation of the form of Fig. 13. Implying that perturbative W exchange will be accompanied by a background, “right-handed”, wee gluon interaction. In QCD_S , with $SU(3)$ color restored, this background interaction will be $SU(3)$ symmetric.

4.2 W Mass Generation

A priori, we anticipate that the existence of Goldstone boson Π 's will lead to the W 's acquiring a mass via the mixing illustrated schematically in Fig. 15.

$$\begin{array}{c} W \\ \text{~~~~~} \end{array} + \begin{array}{c} W \quad \Pi \quad W \\ \text{~~~~~} \end{array} + \begin{array}{c} W \quad \Pi \quad W \quad \Pi \quad W \\ \text{~~~~~} \end{array} + \dots$$

Fig. 15 The Anticipated Mass Generation.

We will show that, in the regge limit, the first interaction term is produced (when $q_{\perp}^2 \rightarrow 0$) by wee gluons in one, or the other, of the scattering pions. The wee gluon anomaly interactions involved are illustrated in Fig. 16.

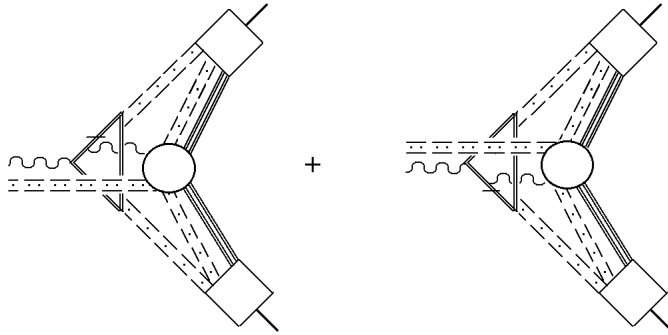


Fig. 16 Anomaly interactions.

For the moment, the quark loop involved can be either sextet or triplet. We will not attempt to identify the higher-order terms in Fig. 15. Identifying the first term will give us sufficient information for our purposes.

With the wee gluon kinematics used in Section 2, the first interaction in Fig. 16 gives, as $q_\perp^2 \rightarrow 0$, the anomaly pole contribution shown in Fig. 17.

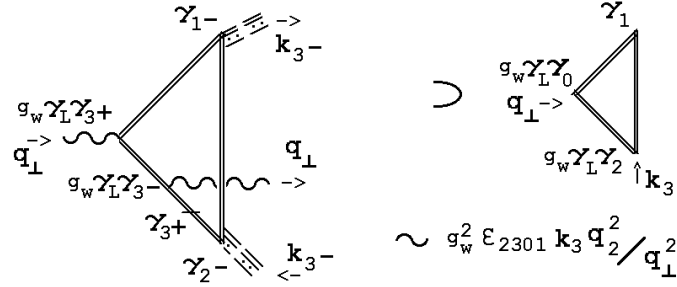


Fig. 17 The anomaly pole contribution.

(Again the notation is the same as in previous diagrams, except that we have introduced $\gamma_L = 1 + \gamma_5$.) The $g_w \gamma_L \gamma_{3\pm}$ couplings appear because the W is exchanged over a large rapidity interval. The γ_1^- and γ_2^- couplings are similarly determined by the wee gluon kinematics.

If we add the two diagrams shown in Fig. 16, and integrate over the wee gluon momentum k_3 , we produce a W mass of the form

$$M_W^2 \sim \frac{q_1^2 + q_2^2}{q_1^2} g_W^2 \int dk_3 k_3 = g_W^2 \int dk_3 k_3 \quad (4.1)$$

That there is actually no pole at $q_\perp^2 = 0$ is consistent with our argument in Section 2 (and Appendix B) that the on-shell residue of an anomaly pole is finite only in an infinite momentum frame. Nevertheless, the quantum numbers at each vertex of the triangle diagram producing the denominator pole are identical to those of the effective triangle diagrams discussed in Section 2. Therefore, the mass generation can be interpreted as due to the direct coupling of a W to a Pion (or pion) just as anticipated in Fig. 15.

As discussed in the previous two Sections, wee gluon momentum factors are generally scaled by a mass factor (M in $CSQCD_S$ or μ in QCD_S). However, because the diagrams of Fig. 16 contain only perturbative W vertices in addition to the wee gluon couplings (with no longitudinal interaction of the form of (2.17)), the wee gluon momentum factor produced by the coupling to the anomaly diagram is not scaled by such a mass factor. As a result, the mass (4.1) that is obtained is a direct reflection of the wee gluon momenta involved together with an overall normalization factor that will be determined by the color factors associated with the sum over all wee gluon couplings to the quark loop involved. Since this color factor will be different for triplets and sextets, we can write the mass obtained from all quark loop interactions

of the form of Fig. 16 as

$$M_W = g_w^2 F_\Pi^2 + \Sigma_{\pi's} g_w^2 F_\pi^2 \quad (4.2)$$

and consider this to be a definition, for our purposes, of both F_Π and F_π .

We will discuss the relative magnitude of F_Π and F_π shortly. First, however, we note that the mass (4.2) appears only for vector bosons with a purely left-handed coupling. The “LLV” structure of the triangle diagram in Fig. 17 gives an anomaly, whereas if the W couplings were purely vector we would have a “VVV” structure and no anomaly. Similarly, if the coupling were purely axial vector we would have an “AAV” structure and, again, no anomaly. Hence, if we now introduce the Standard Model hypercharge gauge field Y , with couplings as discussed above, the above mass generation mechanism will apply also to the left-handed component of Y . We, therefore, obtain exactly the mass generation pattern of the Standard Model and there is no mass for the photon. (Note that photon exchange exchange will be accompanied by a background axial vector wee gluon interaction.)

To discuss the contribution of wee gluon color factors to F_Π and F_π , it will be simpler to make the transition from $CSQCD_S$ to QCD_S . As we have discussed in the previous Section, the wee gluons will no longer be a simple condensate and the W mass generated by wee gluon interactions will be a much more complicated dynamical effect. Nevertheless, we can continue to define F_Π and F_π by (4.2).

The large sextet color factors surely imply that F_Π is much larger than F_π . A common expectation, based on Feynman graph color factors, is that triplet and sextet quark momentum scales for gluon interactions will be related (approximately) by the “Casimir Scaling” rule. This rule would say that F_Π and F_π should be related by

$$C(6) \alpha_s(F_\Pi^2) \sim C(3) \alpha_s(F_\pi^2) \quad (4.3)$$

where $C(3)$ and $C(6)$ are Casimirs for triplet and sextet quarks respectively. For $SU(3)$ there are two Casimir operators which are (representation dependent) multiples of the identity. In terms of the generators G_a , these operators can be written as

$$C_2 = G^2 \sim f_{abc} G_a G_b G_c, \quad C_3 \sim d_{abc} G_a G_b G_c \quad (4.4)$$

and since

$$C_2(6)/C_2(3) = 5/2, \quad C_3(6)/C_3(3) = 7/2 \quad (4.5)$$

we can say

$$C(6)/C(3) \approx 3 \quad (4.6)$$

To apply (4.3) to the real world we must use the physical α_s that is defined via “low-energy” QCD, with the sextet sector integrated out and with the physical quark

masses in place. In this case, if α_s evolves as slowly as is commonly believed (e.g. $\alpha_s(F_\pi^2) \sim 0.4$), the order of magnitude of F_Π will indeed be the electroweak scale! We conclude, also, that the sextet quark Pions will dominate the mass generation for W bosons, as anticipated in Fig. 15, and we can effectively ignore the triplet quark contribution.

We can look at the Casimir scaling rule (4.3) in two complimentary ways. We can use it, as we just did, to obtain directly the relative magnitude of triplet and sextet factors with a momentum dimension, on the basis that this is entirely controlled by the evolution of α_s . More directly, we can say that in going from triplet to sextet graphical contributions, α_s is effectively replaced by $\{C(6)/C(3)\} \alpha_s$. (An explicit example of this is provided by the β -function calculations described in Appendix A.) In this case, we can say that the large factor of F_Π^2 that appears in the W mass results from the color factors associated with the product of the two wee gluon couplings, in the diagrams of Fig. 16, to the sextet quark loop involved. Since, essentially, the same color factors and wee gluon interactions will be involved, we conclude that the wee gluon coupling that provides the coupling of the wee gluon component of the pomeron to a sextet quark loop (in an anomaly pole amplitude) similarly, has the order of magnitude of F_Π . This tells us, as we shall see explicitly in the following, that the pomeron will couple very strongly to the electroweak sector, even though the states are very massive.

5. SEXTET PIONS AT HERA

We begin our discussion of the hard diffractive production of vector bosons (W 's and Z 's) via sextet pions by discussing deep-inelastic diffractive scattering in this Section. As we anticipated in the previous Section, the strong coupling of the sextet sector to wee gluons will be directly evident in the coupling of this sector to the pomeron and, as we show below, we can begin to estimate cross-sections by utilising the generation of a sextet pion via an anomaly pole. Because the produced vector boson carries a large longitudinal momentum and it is longitudinally polarized it has, as we will explain below, an enhanced probability (compared to a transversely polarized vector boson) for decay to a jet pair that are sufficiently close together, in phase space, to appear as a single massive jet. In the kinematical situation at HERA, this is particularly difficult to detect unambiguously. We are encouraged, nevertheless, by the fact that the features of the most dramatic large x and Q^2 event presented[27] by ZEUS, in the original paper highlighting such events, are such that we are able to argue that a Z^0 may, indeed, have been produced.

5.1 Diffractive Hard Interactions

A sextet pion can be directly produced via a hard interaction of the pomeron with a color neutral γ , Z^0 or W^\pm . When no pomeron self-interactions are involved, it should be reasonable to treat the wee gluon component of the pomeron as a condensate, as discussed in Section 3. In this case, as illustrated in Fig. 18, the pomeron can provide directly the wee gluon component that is needed for the sextet pion to appear via an anomaly pole.

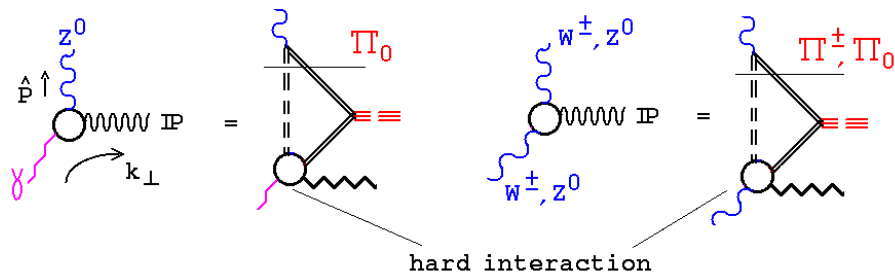


Fig. 18 Hard diffractive interactions.

(We use the same diagrammatic notation as in Section 2.)

At moderate and low Q^2 , deep-inelastic scattering is dominated by photon exchange. To see the sextet pion process, we will require large x and Q^2 and, in fact, Q^2 will be sufficiently large that Z^0 exchange, in the neutral current, and W

exchange, in the charged current will give equally large (or even larger) contributions. In the following we will specifically discuss interactions initiated by a photon and only occasionally refer to the fact that the photon could equally well be a W^\pm or a Z^0 .

The simplest photon interaction that is effectively pointlike at large k_\perp and has the right γ - matrix structure to produce an anomaly pole, is shown in Fig. 19(a).

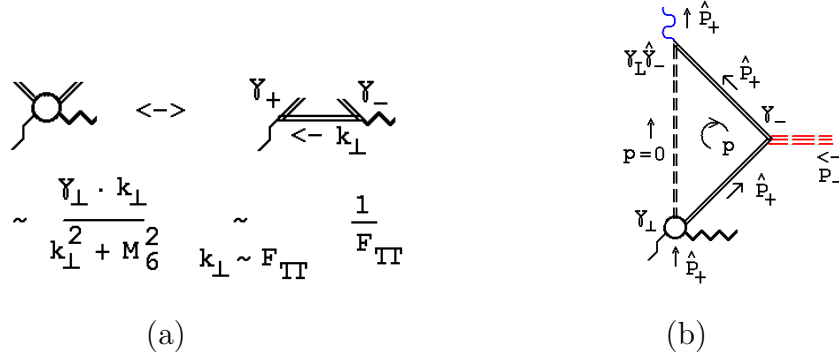


Fig. 19 (a) The hard interaction (b) the anomaly pole diagram.

(M_6 is a dynamical sextet quark mass that we take to be $\sim F_\Pi$.) The resulting anomaly pole diagram is shown in Fig. 19(b). We will see that, in addition to the large k_\perp , the hard gluon in the pomeron must also carry a large light-like momentum.

To obtain an anomaly pole amplitude via a finite on-shell residue we should, in principle, go to the infinite momentum frame of the produced pion. In addition, the anomaly pole description is valid only when when the Π is on mass-shell, with zero mass. However, to produce a Z^0 , and not a Π on mass-shell, it should be reasonable to use the finite momentum anomaly pole amplitude, initially defined close to the Pion mass-shell, and continue that towards the Z^0 pole.

5.2 Diffractive Deep-Inelastic Scattering

The anomaly amplitude shown in Fig. 19(b) gives the contribution to deep-inelastic diffractive jet production illustrated in Fig. 20.

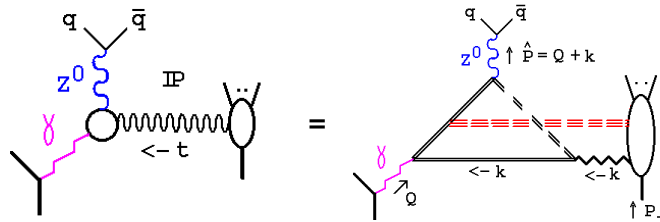


Fig. 20 Deep-inelastic diffractive jet production.

Using the kinematic notation shown in Fig. 19(b) and Fig. 20, we initially take $\hat{P} = Q + k$ to be light-like ($= \hat{P}_+$, as in Fig. 19(b)) but very importantly, because Q is spacelike, the light-cone is not parallel to that defining P_+ and P_- . In this case, with the γ -matrix couplings appearing in Fig. 19(b), the anomaly amplitude has a contribution with the kinematic form

$$\Gamma_{\perp \hat{n}_-} \sim \frac{\hat{P}_+ P_- \hat{P}_+}{P_- \hat{P}_+} = \hat{P}_+ \quad (5.1)$$

where \hat{n}_- is the light-cone vector orthogonal (in the euclidean sense) to \hat{P}_+ . Again there is no anomaly pole. Instead, the effect of this pole is that the amplitude is independent of the wee gluon momentum P_- . Therefore, the anomaly pole wee gluon coupling will produce a simple integral over the wee gluon distribution that, for the reasons discussed in the last Section, we take to be $\sim F_{\Pi}$. Combining (5.1) with this coupling and with the Z^0 propagator and vertices g_w , and extrapolating away from $\hat{P}^2 = 0$ by introducing \hat{P}_- , as a component of $Q + k$, gives

$$F_{\Pi} \hat{P}_+ g_w^2 \frac{(g_{-\nu} - \hat{P}_- \hat{P}_\nu / M^2)}{(\hat{P}^2 - M^2)} = - \frac{\hat{P}_-}{F_{\Pi}} \frac{\hat{P}^2}{\hat{P}^2 - M^2} \delta_{-, \nu} - \frac{\hat{P}_+}{F_{\Pi}} \delta_{+, \nu} \quad (5.2)$$

where M is now M_{Z^0} (but would be M_W if we were discussing W production) and we have used $M = g_w F_{\Pi}$. (All light-cone co-ordinates are now defined relative to the \hat{P} light-cone.) The first term in (5.2) is present as soon as $\hat{P}^2 \neq 0$. It produces a physical, longitudinal, Z^0 .

The second term in (5.2) has no pole, but it is of comparable magnitude away from the pole and (when \hat{P}_- is small) it gives a direct coupling to fermion final states that is proportional to their mass. Note that there is no explicit g_w dependence in (5.2) and when $\hat{P}_+ \sim \hat{P}_- \sim F_{\Pi}$ both terms are $O(1)$. Therefore, at the electroweak scale, the anomaly amplitude produces electroweak final states with no electroweak suppression.

5.3 Comparison With a Jet Amplitude

At first sight, as illustrated in Fig. 19(a), the hard interaction that helps produce the anomaly amplitude gives a suppression $O(1/F_{\Pi})$ at the electroweak scale. However, as we discuss now, this is the natural order of magnitude for a normal two jet amplitude that does not involve sextet pion production.

We consider the two jet amplitude involving gluon exchange shown in Fig. 21(a), and consider the two production vertices shown in Fig. 21(b). (Once again the photon could be replaced by either a Z^0 or a W^{\pm} .) The first vertex shown is a lowest-order

Figure 1 consists of two parts, (a) and (b), each showing Feynman diagrams for the production of a Z boson and a top quark pair.

Part (a) shows a diagram where a gluon (represented by a wavy line) splits into a quark-antiquark pair (q, \bar{q}). The quark and antiquark then annihilate to produce a Z boson (represented by a vertical oval). The Z boson then decays into a top quark and an anti-top quark (t, \bar{t}). The incoming gluon has momentum Q , and the outgoing top quark and anti-top quark have momenta p_+ and p_- respectively. The total momentum of the Z boson is $\hat{p} = Q + k$.

Part (b) shows a diagram where a quark and an antiquark (q, \bar{q}) annihilate to produce a Z boson (represented by a vertical oval). The Z boson then decays into a top quark and an anti-top quark (t, \bar{t}). The incoming quark and antiquark have momenta q and \bar{q} respectively, and the outgoing top quark and anti-top quark have momenta p_+ and p_- respectively.

The second difference between the jet amplitude and the anomaly amplitude is that a regular gluon (parton) vertex replaces the pomeron vertex (that is the reggeized gluon plus wee gluons vertex), giving a reduction by a factor of $\approx 1/3$ in the amplitude. This will be compensated, in part, by the appearance of a sextet quark coupling (relative to a triplet coupling). Therefore, when all the momenta involved are electroweak scale in magnitude, the diffractive production of jet pairs via Z^0 production will give a comparable cross-section to that for conventional (non-diffractive) two jet production.

5.4 The Angular Distribution of Produced Jets and Leptons

34

If we denote the (four-) momentum vectors of the produced fermions by X and Y , then if the Z^0 momentum is

$$P_{Z^0} = (P_+ + P_-, P_+ - P_-, 0, 0), \quad \text{where} \quad 4P_+P_- = M^2 \quad (5.3)$$

the most general form for X and Y is

$$\begin{aligned} X &= (\lambda P_+ + (1 - \lambda)P_-, \lambda P_+ - (1 - \lambda)P_-, p_\perp, 0) \\ Y &= ((1 - \lambda)P_+ + \lambda P_-, (1 - \lambda)P_+ - \lambda P_-, -p_\perp, 0) \end{aligned} \quad (5.4)$$

where $0 \leq \lambda \leq 1$. The mass of both fermions is given by

$$m_f^2 = 4\lambda(1 - \lambda)P_+P_- - p_\perp^2 = \lambda(1 - \lambda)M^2 - p_\perp^2 \quad (5.5)$$

This notation will be convenient for our purposes, even though it obscures the fact that we could obtain all momenta via a boost from the rest frame of the Z^0 . In this frame, the only variable would be the angle between the transverse momenta of the fermion pair and the direction in which the Z^0 is to be boosted. This is, of course, why p_\perp and λ are related via (5.5).

We consider first a transverse coupling which, for the purpose of γ -matrix manipulations, we write in the form

$$\langle Y | n_\perp \cdot \gamma_\perp | X \rangle \quad (5.6)$$

where n_\perp is a unit transverse vector. Suppose, first, that P_+ is so large that both P_- and p_\perp can be neglected. Using the Dirac equation for $|X\rangle$ then gives

$$\langle Y | n_\perp \cdot \gamma_\perp | X \rangle \sim \frac{\lambda}{1 - \lambda} \langle Y | n_\perp \cdot \gamma_\perp | X \rangle \quad (5.7)$$

$$\implies \langle Y | n_\perp \cdot \gamma_\perp | X \rangle = 0 \quad (5.8)$$

except, possibly, when $\lambda = (1 - \lambda) = 1/2$. Not surprisingly, we have to add transverse momentum in order to get substantial information about how a transversely polarized Z^0 will decay.

If we repeat the above manipulation keeping the transverse momentum dependence we obtain

$$\begin{aligned} \langle Y | n_\perp \cdot \gamma_\perp | X \rangle &\sim \langle Y | n_\perp \cdot \gamma_\perp (\lambda \gamma_- P_+ + \gamma_\perp \cdot p_\perp) / m_f | X \rangle \\ &\sim \frac{\lambda}{(1 - \lambda)} \langle Y | n_\perp \cdot \gamma_\perp | X \rangle + \frac{(1 - 2\lambda)}{(1 - \lambda)} \langle Y | p_\perp \cdot n_\perp | X \rangle / m_f + \dots \end{aligned} \quad (5.9)$$

The additional terms cancel if we add the corresponding equation obtained by reversing the roles of λ and $(1 - \lambda)$. (Note that $(1 - 2\lambda)$ changes sign under $\lambda \leftrightarrow (1 - \lambda)$ but, also, $m_f \leftrightarrow -m_f$.) We then obtain the simple result

$$\langle Y | n_{\perp} \cdot \gamma_{\perp} | X \rangle \sim - \langle Y | p_{\perp} \cdot n_{\perp} | X \rangle / m_f \quad (5.10)$$

We learn from (5.10) that a transverse Z^0 decays to fermions with transverse momenta determined by the polarization. The amplitude is a maximum when $|p_{\perp}|$ is a maximum which, from (5.5) occurs when $\lambda = 1/2$. In this case, the fermions symmetrically carry one half of the light cone momenta of the Z^0 . It is a smooth maximum, however, and so there is a significant probability that the Z^0 will decay into an asymmetric configuration.

If we repeat the above discussion for the longitudinal polarization we obtain a non-zero contribution already in the first manipulation, i.e.

$$\begin{aligned} \langle Y | \gamma_+ | X \rangle &\sim \langle Y | \gamma_+ \lambda \gamma_- P_+ / m_f | X \rangle \\ &\sim \frac{\lambda}{1 - \lambda} \langle Y | \gamma_+ | X \rangle - 2\lambda \langle Y | P_+ | X \rangle / m_f \end{aligned} \quad (5.11)$$

giving

$$\langle Y | \gamma_- | X \rangle \sim - \frac{2\lambda(1 - \lambda)}{m_f(1 - 2\lambda)} \langle Y | P_+ | X \rangle \quad (5.12)$$

Now the symmetric case, with $\lambda = 1/2$, is strongly enhanced. Although, because terms that are non-leading as $P_+ \rightarrow \infty$ will also be singular as $\lambda \rightarrow 1/2$, we can use (5.12) only if we stay away from $\lambda = 1/2$. It is, nevertheless, sufficient for us to conclude that, at large momentum, the symmetric configuration with two jets (or leptons) close together in phase space is enhanced for a longitudinal Z^0 decay, compared to the transverse case. In general, the final result may often look like a broad single jet.

5.5 HERA Kinematics

For most of our discussion we will take both the proton and the positron to be massless. We denote the momentum of the proton beam by E_p and the momentum of the positron beam by E_e . If we write the photon (or Z^0 , or W^{\pm}) momentum as

$$Q = (Q_+ + Q_-, Q_+ - Q_-, Q_{\perp}) \quad (5.13)$$

then the light-cone components Q_+ and Q_- are determined, at fixed x and Q^2 , by the mass-shell condition for the scattered positron, i.e.

$$0 = 4p_- Q_+ - Q^2 \quad (5.14)$$

and

$$x = \frac{Q^2}{4P_+Q_-} \quad (5.15)$$

Solving for Q_\perp^2 , we obtain

$$Q_\perp^2 = Q^2 - \frac{Q^4}{Sx} = (1-y)Q^2 \quad (5.16)$$

where $S = 4P_+p_-$ and $xyS = Q^2$.

(5.16) shows that large Q_\perp requires both large x and Q^2 . With $E_p = 820$ GeV and $E_e = 27.5$ GeV (the original HERA values) we can obtain $Q_\perp \sim 100$ GeV with $Q^2 \sim 30,000$ GeV² and $x \sim 0.5$. However, if (in the notation of Fig. 20) we also require that $k_\perp \sim 100$ GeV and $\hat{P}^2 \sim M_{Z^0}^2$ then, not surprisingly, it is very difficult to have all conditions satisfied. First, it is necessary for k to have a very large light-cone component to put the Z^0 on-shell. We then find that to keep the diffractively excited proton state physical we must have $|k^2| = |t| \gtrsim 2k_\perp^2 \sim 20,000$ GeV². In this case, the jet cross-section we are comparing with will be far too small to be observable.

5.6 Small t Scattering

We can extend the foregoing discussion with an argument that we will also apply to other diffractive amplitudes in later Sections. According to our analysis, the QCD_S pomeron is essentially a regge pole and so has, approximately, the factorization properties of a regge pole all the way from electroweak scale values of $|t|$ down to $|t| \sim 0$. The regge behavior is manifest at large $|t|$ via the reggeized gluon that gives the kinematic properties of the hard pomeron that we have been discussing and this will match smoothly with a soft pomeron regge pole as $|t|$ decreases. (Note that t can be small even though a large light-like momentum is exchanged.) Since we anticipate that the “non-perturbative” $\gamma Z^0 \text{IP}$ vertex is entirely due to electroweak scale dynamics it should vary only slowly with $|t|$ (with a scale determined by F_Π). However, the proton/pomeron coupling will be the normal hadronic coupling and will increase exponentially fast as $|t|$ decreases. It is difficult to know how large this increase will be, since there are no measurements of this coupling for $|t| \sim 20,000$ GeV² ! We do know that the cross-section for proton elastic scattering, which involves the square of the coupling that we are interested in, decreases by five orders of magnitude between zero and $|t| \sim 1$ GeV², and by another five orders of magnitude between $|t| \sim 1$ GeV² and $|t| \sim 10$ GeV². The mass-shell condition for the proton to scatter elastically, with a large longitudinal momentum exchanged, is $|t| \lesssim 2-3$ GeV². With the increase by orders of magnitude as $|t|$ decreases, if we are also close to the Z^0 pole, the resulting cross-section may well be observable.

5.7 What Can be Seen at HERA ?

In the original ZEUS paper[27] five events were highlighted which all had relatively large x and Q^2 . We have identified an electroweak scale $|Q_\perp|$ as necessary for sextet pion Z^0 production and four events had $|Q_\perp| \gtrsim 100$ GeV. Although subsequent ZEUS data[32] appear to show that the e^+p cross-section at large x and Q^2 (up to, and including, $Q^2 = 30,000 \text{ GeV}^2$) is not substantially above that predicted by the Standard Model, H1 data give a different impression. The published H1 cross-section[33] for the neutral current at $Q^2 = 30,000 \text{ GeV}^2$ (and the charged current at lower Q^2) seems to be significantly above the Standard Model value. Therefore, it remains possible that some fraction of the original five ZEUS events (particularly at $Q^2 > 30,000 \text{ GeV}^2$) and, presumably, subsequently observed events, are due to a non Standard model process. In fact, as we now discuss, only the largest Q^2 event clearly has a high probability to have resulted from Z^0 production.

In each event there is a clear jet and the essential question is whether it could have been a massive jet produced by a Z^0 . We will make use of the fact that two, a priori independent, reconstruction methods are used to measure both Q^2 and x and the results from both are quoted separately for each event. The first method, called the “double-angle” (DA) method uses only the measured angles of the jet (γ) and the electron (θ_e), together with the formulae

$$x_{DA} = \frac{E_e}{E_p} \frac{\sin\gamma}{(1 - \cos\gamma)} \frac{\sin\theta_e}{(1 - \cos\theta_e)}, \quad y_{DA} = \frac{\sin\theta_e(1 - \cos\gamma)}{\sin\gamma + \sin\theta_e - \sin(\gamma + \theta_e)}, \quad (5.17)$$

and $Q_{DA}^2 = sx_{DA}y_{DA}$. The other “positron” method uses only the measured positron energy E'_e and the angle θ_e , together with the formulae

$$x_e = \frac{E_e}{E_p} \frac{E'_e(1 + \cos\theta_e)}{2E_e - E'_e(1 - \cos\theta_e)}, \quad y_e = 1 - \frac{E'_e}{2E_e} (1 - \cos\theta_e) \quad (5.18)$$

and, again, $Q_e^2 = sx_e y_e$. Although this second method is much more direct, because of the difficulty of measuring E'_e reliably, the double angle method is generally regarded as more reliable for discussing large Q^2 deep-inelastic events.

The double angle method is predicated[34] on the assumption that the jet mass can be neglected. As a result, (5.17) correctly gives x and Q^2 only when the jet is (at least approximately) massless. Therefore, whether or not, there is agreement between the two methods can be regarded as an indirect test of the smallness of the jet mass. In fact, for all but the largest Q^2 event, there is no significant disagreement.

5.8 The Largest Q^2 Event

This event is shown in Fig. 22. The jet is clearly very broad and, in fact, the

results for Q^2 and x obtained from the two reconstruction methods differ significantly, with the differences being outside of the quoted errors.

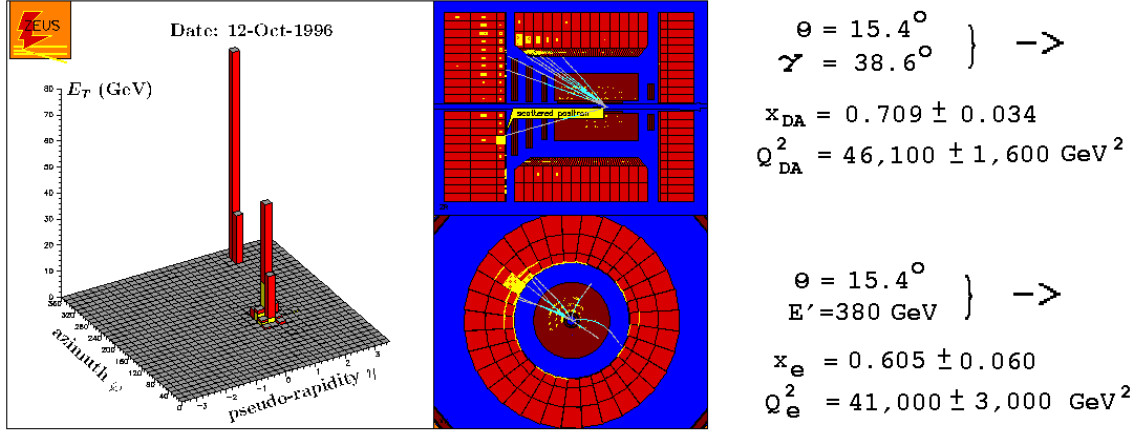


Fig. 22 The largest Q^2 ZEUS event.

If we reconstruct the full four-momentum Q from (5.13)-(5.16) we obtain

$$Q_{DA} = (-399, -439, -113, 0) \quad (5.19)$$

and

$$Q_e = (-352.5, -393.5, 101, 0) \quad (5.20)$$

We can regard the double-angle method as projecting the experimentally measured calorimeter energies and momenta onto the combination of a massless jet and an additional momentum projected onto the measured direction of the positron. In effect, this is what is done by the process of eliminating the energy of the positron and assuming that only the angle is well determined experimentally. The jet angle γ is determined directly (under the assumption that the jet is massless). Following the procedure used in the ZEUS paper we determine the jet energy by using the fact that p_\perp is approximately conserved (as is recorded in Fig. 22). As a result, the p_\perp of the jet must balance that given by Q_e . With $\gamma = 38.6^\circ$, this determines the four-momentum of the (assumed to exist) massless jet to be

$$P_j = (167, 126.5, 101, 0) \quad (5.21)$$

Taking the directly measured Q_e to be correct, the additional momentum projected along the positron direction is

$$Q_e - Q_{DA} = (46.5, 45.5, -12, 0) \quad (5.22)$$

Adding this back to P_j to, potentially, obtain the true four momentum of the produced hadronic state we obtain

$$P_j + Q_e - Q_{DA} = (213.5, 172, 89, 0) \quad (5.23)$$

which has a mass squared of

$$8,077.25 \text{ GeV}^2 = (89.9 \text{ GeV})^2 \quad (5.24)$$

suggesting that a massive Z^0 jet was indeed produced. The production angle would have been $\gamma_{Z^0} = 27.4^\circ$ which is large enough to be detected only because Q^2 is so large.

If we compute the momentum transfer k using (5.23) for the momentum \hat{P} of the Z^0 we obtain

$$k = P_{Z^0} - Q_e = (566, 565.5, 12, 0) \quad (5.25)$$

implying (more exactly than is surely justified by all the reconstruction involved) that the squared momentum transfer may have indeed been small. Thus allowing the interpretation of the event as diffractive Z^0 production.

5.9 Other Events

It will be very interesting to determine whether the foregoing analysis can reveal further HERA events that might be consistent with diffractive Z^0 production. Although the H1 events, that were presented in the paper[35] that was contemporaneous with the ZEUS paper, carried large Q^2 they were selected with different criteria and were presented from a different viewpoint. There was an emphasis on the possibility of a large mass intermediate state in the electron + jet channel that led to the presentation of the kinematics of the events in a way that makes it impossible to directly apply our analysis. Also the search for a large mass intermediate state produced an emphasis on large y , and hence low Q_\perp^2 , that is counter to our purpose. In particular, the two largest Q^2 events presented (with $Q^2 \sim 31,000 \text{ GeV}^2$) both had relatively small x (~ 0.45) and consequently had lower Q_\perp^2 ($\sim 80 \text{ GeV}$) than we would prefer for our analysis.

Presumably, both ZEUS and H1 have further candidate events from runs subsequent to 1997. However, cross-sections for $Q^2 > 30,000 \text{ GeV}^2$ have yet to be published, as have any corresponding event pictures.

6. SEXTET PHYSICS AT FERMILAB

6.1 Single Diffraction

The interactions shown in Fig. 18 will also take place in a hadron collider when a Z^0 , W^\pm , or photon is emitted from a quark in a hadron. Unfortunately, it will be very difficult to isolate these processes because of the small cross-section involved. However, as in our discussion of deep-inelastic scattering in the previous Section, the t dependence of the pomeron/hadron vertex implies there should be a “relatively large” forward amplitude. In fact, this interaction could explain the push towards larger rapidities, that is apparently observed[36] at the Tevatron, when a W^\pm or Z^0 is produced in association with a large E_T jet.

Diffraction production of vector boson pairs might also be possible, although it is not clear whether the corresponding anomaly pole vertices exist. Apparently[37], there is already an anomalously large (non-diffractive) W pair cross-section at the energy of the $S\bar{p}pS$ collider. Since, as we discuss in the next Section, we expect this cross-section to be really large at the LHC, it seems that an “anomalous” (although still relatively small) cross-section should surely be observed at the Tevatron. A sextet pion coupling might then give an unexpectedly large single diffractive component. A complication is that detection of events in which one of the pair decays hadronically is much more difficult at the Tevatron than it was at the $S\bar{p}pS$ because of the large background from the QCD production of W (or Z) plus two jets. In addition, the vector boson pairs will be produced with much greater momentum at the Tevatron (than at the $S\bar{p}pS$) and so the problem of the close together decays of longitudinal bosons will be much more significant.

Other anomalous events, related to the single diffractive interactions, may also be observed. In particular, a connection between diffractive cross-sections and events with twice the average multiplicity density (in rapidity) is required by the AGK cutting rules. In addition, the Wilson lines attached to sextet quarks should also generate higher associated multiplicities than triplet quark lines. Anomalously low multiplicity events may anticipate the higher energy rapidity gap cross-sections that we expect to appear.

6.2 Double Pomeron Exchange at the Tevatron

Double pomeron production of W^\pm and Z^0 pairs which, as we discuss in the next Section, we expect to be a very clean signal of sextet quark physics at the LHC, is (probably) inaccessible kinematically at the Tevatron. However, a Z^0 can also pair with a photon to give a state with zero sextet quark flavor. Since double pomeron production of $Z^0\gamma$ is accessible kinematically, although there is not an obvious anomaly

pole vertex, there could be a significant (although small, because an electromagnetic coupling is involved) anomalous cross-section for this process at the Tevatron. Since there are two hadron/pomeron couplings there should also be a major increase of the cross-section at smaller t . Assuming that the photon can simply play the role of introducing sextet quark quantum numbers, it need not carry electroweak scale transverse momentum.

6.3 The η_6 , $t\bar{t}$, and Large E_T Jets.

We turn now to non-diffractive sextet quark physics that might be seen (or may have already been seen) at the Tevatron.

As illustrated in Fig. 23, the η_6 has two anomaly couplings to wee gluons in $CSQCD_S$. There is both a $Q\bar{Q}$ and an $SU(2)$ singlet gluon coupling (where the gluon has a non-leading helicity). Therefore, in QCD_S , the η_6 mixes with a pure glue state



Fig. 23 Anomaly couplings for the η_6 .

and, as a result, we expect that it will have an electroweak scale mass, with the sextet quark and antiquark carrying electroweak scale constituent masses. The η_6 will also mix, via the gluon state, with the triplet flavor singlet (the η_3) that will be dominated by $t\bar{t}$ at the electroweak scale.

We anticipate, therefore, that the η_6 has an electroweak scale short-distance component which carries octet color that is compensated by wee gluons. This short distance component can be produced via gluon production and, since sextet quarks are stable, it will decay, primarily, through $t\bar{t}$. Assuming that the major disparity in scales leads to a minimal dynamical role for the wee gluons in the process, $t\bar{t}$ production at Fermilab could be due to the η_6 , and could be, essentially, “perturbatively” calculable. This would imply, however, that $m_{\eta_6} \sim “2m_t”$.

That top production is due to resonance production would, of course, resolve the paradox that the production of a confined, colored, quark can, apparently, be observed experimentally. Theoretically, and “philosophically”, it would surely be attractive if an electroweak scale mass, i.e. $2m_t \sim 350 \text{ GeV}$, is explained as the (dynamical) mass of a sextet quark/antiquark bound state, rather than as (twice the value of) a lagrangian parameter of the triplet quark sector. Whether a well-determined top quark “mass” should still be, experimentally, identifiable is not clear.

Within QCD_S , the existence of a non-perturbative QCD sector above the “mass” of the top quark makes it very unlikely that the concept of a perturbative,

electroweak scale, current quark mass can be well-defined enough to be directly measured. There would be a large dynamical mass generated above the electroweak scale that, most likely, would make the concept of the current quark mass very elusive. Alternatively, if we identify the η_6 as responsible for top production then we can identify m_t as the sextet quark constituent mass scale. This would imply that the sextet neutron N_6 has a relatively low mass of $500 - 600 \text{ GeV}$. As we will discuss in the next Section, this maximises the possibility that the Cosmic Ray spectrum knee is associated with the appearance of sextet quark states.

As detailed in Appendix A, the contribution of the sextet quark doublet to the QCD β -function is equivalent to the contribution of ten triplet quarks. Consequently at the scale where (non-chiral) sextet quarks enter the dynamics, they will halt the evolution of α_s entirely. If the top quark mass is actually the sextet constituent mass scale, as we have suggested, then the evolution of α_s will halt at $E_T \sim m_t$. In Fig. 24(a) we show a CDF analysis[38] which translates the observed (Run 1) jet excess at large E_T into the (non-)evolution of α_s . As can be seen, α_s does indeed stop evolving just at $E_T \sim m_t$.

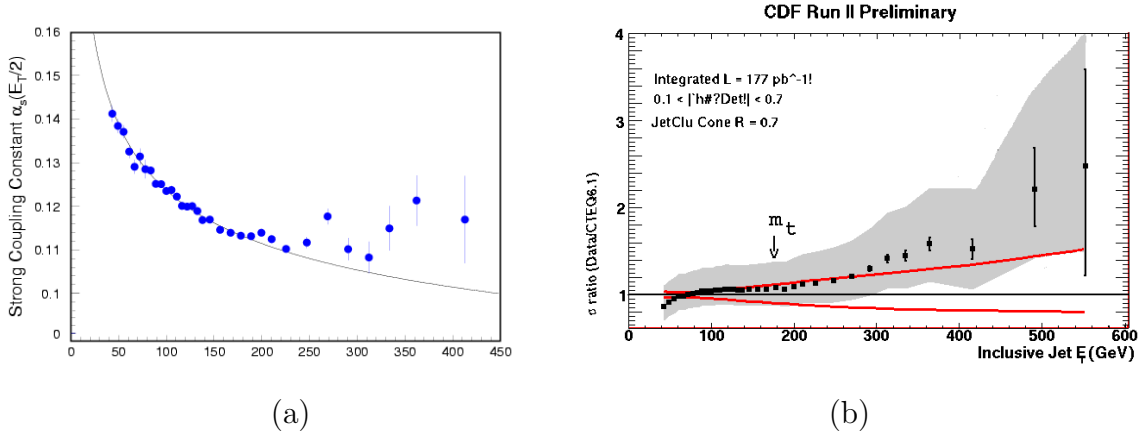


Fig. 24 CDF jet cross-section measurements.

Measurement of the jet cross-section in Run 2 appears, at present, to be entangled by the very real problem of systematic experimental errors. In Fig. 24(b) we show the current comparison of data with theory[39]. Note that “theory” in this case includes a gluon distribution that was chosen to best fit the Run 1 excess cross-section. As can be seen, if we ignore the experimental error problem, the data again pull away from theory, for $E_T \sim m_t$ upwards, with the effect clearly growing with E_T .

It seems possible, if not probable, that above the electroweak scale, QCD jet physics is breaking down in just the manner that we would expect from QCD_S . Indeed, if the top mass has the significance that we have just discussed, then the sextet sector has fully entered the theory at this scale. In addition to halting the

evolution of α_s , the increasing entry of sextet sector states into the dynamics should imply that the “excess” continues to grow as E_T increases. Indeed, we would expect that in the highest E_T excess region there is an enrichment of longitudinal W^\pm and Z^0 jets with $M_{jet} \approx M_{W/Z}$. As we discuss in the next Section, at the LHC such events will have become a major part of the cross-section.

6.4 Non-perturbative Decay Modes

If the η_6 is indeed responsible for $t\bar{t}$ production, then we would also expect to see “non-perturbative” decay modes. To discuss these modes, the best we can do is to exploit the parallel between the $\{\Pi^\pm, \Pi^0, \eta_6\}$ sextet states, corresponding to $\{W^\pm, Z^0, \eta_6\}$, and the familiar $\{\pi^\pm, \pi^0, \eta\}$ triplet quark states. Although the width should be large, if we take $m_{\eta_6} \sim 2m_t \sim 350\text{GeV}$, the relative couplings and masses of the vector mesons, and the photon, imply that the primary non-perturbative decay mode should be (in parallel with $\eta \rightarrow \pi^+ \pi^- \pi^0$)

$$\eta_6 \rightarrow W^+ W^- Z^0 \quad (6.1)$$

which, when $Z^0 \rightarrow b\bar{b}$, would give the same final state as $t\bar{t}$. The next most significant mode

$$\eta_6 \rightarrow Z^0 Z^0 Z^0 \quad (6.2)$$

(in parallel with $\eta \rightarrow \pi^0 \pi^0 \pi^0$) should have a smaller branching ratio, because of the larger Z^0 mass. In addition, (6.2) would be indistinguishable from (6.1) when the Z^0 's decay hadronically, as they do most of the time. Because the η_6 mass is so large, decay modes involving an electromagnetic coupling, such as

$$\eta_6 \rightarrow W^+ W^- \gamma, \quad Z^0 Z^0 \gamma, \quad Z^0 \gamma \gamma, \quad \gamma \gamma \quad (6.3)$$

would be expected to have smaller branching ratios but should be present at some level.

Unfortunately, because the non-perturbative decay modes proceed via sextet pion interactions, the produced vector mesons will be longitudinally polarized and so, as we discussed in the previous Section, when they carry large momentum they will have close together jet and lepton decay modes that are more difficult to detect.

7. DARK MATTER, COSMIC RAY PHENOMENA, AND LARGE CROSS-SECTION LHC PHYSICS

If the sextet sector exists, the LHC will most probably be the discovery machine, at least as far as accelerator physics is concerned. In the next Section, we will give direct theoretical arguments for effects that should be seen at the LHC. However, we will not be able to predict, theoretically, the magnitude of the major phenomena we expect with any great certainty. However, if there is “a major change in the strong interaction above the electroweak scale”, it surely should be visible in Cosmic Ray physics and, more generally, in other cosmic phenomena. As we now discuss, there are candidate phenomena of this kind and, if they are interpreted as we will suggest, they indicate that large cross-section effects are to be expected at the LHC. We first give a brief, qualitative, discussion of why we expect the sextet sector to appear with high-energy cross-sections that are larger than hadronic in size and what we expect the major effects of these cross-sections to be.

7.1 Larger Than Hadronic Size Cross-Sections

If QCD_S existed in isolation, without the electroweak sector, then, because of the larger Casimirs, the sextet sector would constitute a stronger coupling sector of the theory. Just how significant the casimir effect is, we do not know. In general, it is clearly present in perturbation theory but is less significant in conventional non-perturbative formalisms. In QCD_S , because of the “almost perturbative” form of confinement that is present, we expect the effect to be maximal. Most importantly, though, we do not know how the wee gluon distribution contributes to the pomeron couplings that determine the size of asymptotic cross-sections, although sextet couplings should surely be larger. Therefore, the best we can say is that sextet pions will be massless and have asymptotic cross-sections that are (probably considerably) larger than their triplet counterpart. The sextet nucleon mass scale will be larger than the triplet scale but, nevertheless, sextet nucleon asymptotic cross-sections should also be larger. In general, therefore, although the asymptotic mass scale will be much larger, the size of asymptotic cross-sections, including multi-pomeron cross-sections, should be larger for the sextet sector, than the triplet sector, in QCD_S .

Adding the electroweak sector transforms the massless sextet pions into massive vector mesons. Effective current quark masses also have to be added. At asymptotic energies neither effect should matter, but such effects do matter for determining the scale above which asymptotia sets in. In addition, if we start (in the real world) with initial triplet states we will only be able to produce the large cross-section sextet states via multiple gluon exchange and therefore, to obtain large cross-sections, via the pomeron. This does not mean, however, that only double pomeron production processes can be involved. If the double pomeron amplitude for the production of a

sextet state, such as the W^\pm pair amplitude shown in Fig. 25(a), is large (as we show in the next Section) then the associated “cut-pomeron” amplitude, shown as the first diagram in Fig. 25(b), should also be large. (This amplitude is, however, entirely non-perturbative in that it can not be obtained by an anomaly pole method.)

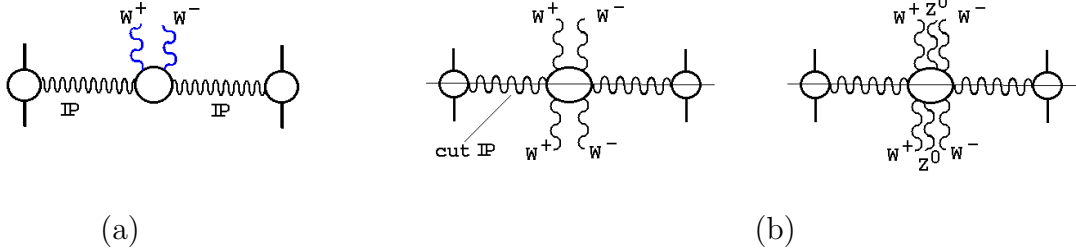


Fig. 25 (a) The double pomeron W pair amplitude (b) cut-pomeron amplitudes.

The cut-pomeron amplitude describes the full, central region, inclusive cross-section for production of a W^\pm pair. Like the total cross-section, a significant part of the inclusive cross-section should be describable by pomeron exchange, even when only a relatively small rapidity range is effectively available for one cut-pomeron or the other. Therefore, when the cut-pomeron amplitude is large it implies that W^\pm pairs (and, similarly, Z^0 pairs) will be strongly, and multiply, produced inclusively across a larger part of the rapidity axis than is covered by the double pomeron produced state. The second cut-pomeron amplitude shown in Fig. 25(b) describes the inclusive production of three boson states which requires, of course, a bit more energy, and so on for higher cut-pomeron amplitudes. Once there is enough energy for cut-pomeron exchange to begin describing significant production of the sextet sector then the larger cross-sections of this sector should imply that sextet states actually come to dominate the inelastic (triplet state) hadronic cross-section at a (not too much) higher energy.

We expect, therefore, that the initial “major change in the strong interaction above the electroweak scale” will be that multiple vector boson states are produced, with large cross-section, across most (but not all) of the rapidity axis - in close analogy with pion production at much lower energies. Sextet nucleon production will set in at higher energies, depending on the mass of these states. If the pomeron provides the gateway to the asymptotically dominant sextet sector, then we could expect that to produce a sextet state with mass M requires at least $\sqrt{S} > 10M$ and so if $M \sim 400 \text{ GeV}$ (to be safely above the threshold for vector boson pair production) then we would need $\sqrt{S} > 4 \text{ TeV}$ - which is just above the Fermilab energy.

7.2 The N_6 and Dark Matter

That the (triplet quark) proton is lighter than the neutron is entirely due to the fact that the current mass of the u quark is less than that of the d quark.

Electromagnetic effects, alone, would make the proton heavier. Because of the absence of hybrid triplet/sextet states, the lightest of the sextet nucleons will be stable. However, sextet quark current masses must be zero. If not, sextet pions would be massive and could not mix with the massless W and Z states to give them masses, as discussed in Section 5. Therefore, the sextet nucleon mass difference has to be entirely electromagnetic in origin, and so it is the N_6 that is stable. If the sextet quark dynamical mass is given by the top quark mass, as discussed in the last Section, then the N_6 mass should be $\approx 500 \text{ GeV}$ and the P_6 mass should be just a little higher. Since triplet and sextet quarks do not combine to form bound states it is, presumably, reasonable to assume that sextet nucleons also do not form bound states with triplet nucleons. More particularly, perhaps, if pion exchange provides the binding force for nucleons to form nuclei, the distinct quark content of sextet and triplet nucleons implies that there is no common “pion” that can bind them.

The N_6 is, therefore, neutral, stable, and (because of the dominance of sextet states) will be the dominant, heavy, stable state produced in high energy cross-sections. Consequently, it will be dominantly produced in the high energy interactions that are believed to have been responsible for the formation of the early universe. If it does not form bound states with normal quark matter it will abundantly form cold dark matter, in the form of (sextet) nuclei, clumps, etc. (Perhaps sextet pions can exist inside sextet nuclei and provide the binding force.) As a result, the existence of the sextet nucleon sector provides a natural explanation for the dominance of dark matter in the universe. Conversely, once we establish that the N_6 will form dark matter, the dominance of dark matter in the universe can be regarded as evidence confirming that sextet quark states dominate high energy cross-sections.

The dominance of dark matter in the universe does not tell us at what energy scale this dominance appears in total cross-sections. Specific evidence for the relevant scale is, however, provided by the cosmic phenomenon that we discuss next.

7.3 The Knee in the Cosmic Ray Spectrum

The “knee” in the cosmic ray spectrum is an extraordinary, well-established and very well-known, phenomenon. As shown in Fig. 26(a), it appears as a break in the slope of the spectrum that stands out, as a distinctive feature, as the energy increases over some ten orders of magnitude and the flux decreases by thirty orders of magnitude. In first approximation, there is one single slope as the energy increases from 10^{10} eV to 10^{16} eV and a second slope as the energy increases from 10^{16} eV to 10^{20} eV . It is called the knee because, as is clear from the larger scale plot shown in Fig. 26(b) (normalized by the low-energy slope), it is not simply a break in slope but rather a “bump” in which, for a short energy range, it looks like the slope has decreased before it settles at an increased value.

It is widely believed by cosmic ray physicists that the origin of the knee is

cosmic, even though there is no consensus on what the cause could be.

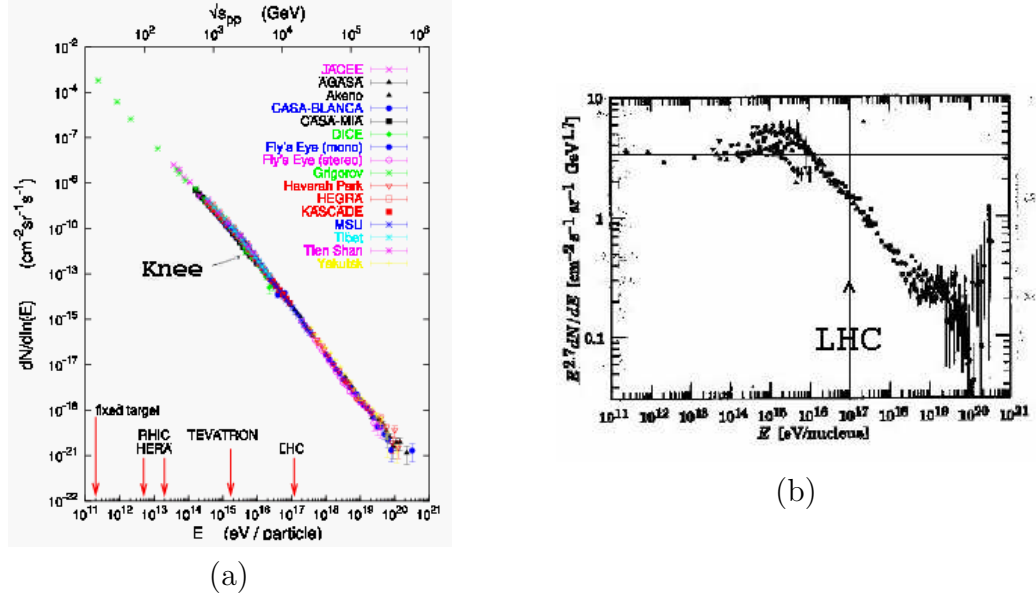


Fig. 26 (a) The full cosmic ray spectrum (b) The knee.

A priori, it seems almost inconceivable that a conspiracy of external phenomena could produce such a pronounced local effect, in a spectrum that (naively at least) is arriving from all directions and all distances of the universe. It seems far more plausible that the cause of the effect is in the atmospheric interaction. Indeed, right from its earliest discovery, it was suggested[40] that the knee could be the threshold for a new interaction that produces (stable or relatively stable) neutral particles which are not observed in the ground level detectors. This would produce an underestimation of the shower energy above the threshold and would lead to a pile-up of events below the threshold energy which, together with a depletion of the spectrum above the threshold, would be observed as a “knee”. However, the major part of the cross-section has to be affected by this threshold. Since there was no serious idea what the neutral particle(s) could be and there was no reason to expect such a dramatic effect in the strong interaction, particularly after the discovery that this interaction is described by QCD, there was no general acceptance of the proposal.

We first proposed that the sextet threshold could be responsible for the knee some time ago[18]. In the meantime, other authors have emphasized the difficulty of explaining the knee as an effect of cosmic physics and have made various proposals[40, 41, 42] for a threshold effect that could be involved. That a large fraction of the cross-section (increasing as the energy increases) has to be involved, is a problem for all

threshold proposals. Because the data from different experiments do not agree about the absolute value of the flux and also cover different energy ranges, it is difficult to be sure exactly where the threshold should be and how much of the cross-section has to be involved. It is clear, however, that the threshold should be below the LHC energy and that the physics involved should be visible at the LHC as a significant part of the hadronic cross-section ($\sim 10\text{-}20\%$). As the discussion in **7.1** shows, the sextet sector threshold has (perhaps uniquely) the potential, at least, to play this role.

The the prolific production of vector bosons, will increase the average transverse momentum of events enormously and lead to such an increase of the shower spread that a much greater fraction (than expected) of the shower particles will be undetected. At the LHC, ten or more vector bosons could be produced, kinematically, via the cut-pomeron cross-section. The major consequence will, of course, be a huge increase of the large E_T jet cross-section. (The effective increase due to the non-evolution of α_s will be just a small part of this effect). There will also be marked changes in the distributions of leptons produced. In particular, there will be a much larger fraction of (undetected) neutrinos in the ground level particles. The production of “dark matter” (sextet neutron/antineutron pairs) will straightforwardly take away undetected energy and the effect will be maximal if the sextet neutron mass is as low as possible. At higher energies the inclusive production of N_6 pairs will surely become more and more significant and, necessarily, be a major contribution to the loss of detected energy by most of the total cross-section.

It is interesting that the production of N_6 pairs is not so different from the original proposal[40] of the production of neutrals to explain the knee. Of course, the existence of dark matter was unknown and the link between the two phenomena, that we are proposing, could not have been imagined.

7.4 Cosmic Ray Dijets and Ultra High Energy Events

There are a number of distinct effects that have been seen in cosmic ray showers with energies above the knee, for example those discussed in [40]. Collectively, they all suggest that new physics appears above the knee. We catalogued the effects, and offered explanations of the phenomena involved, in [18]. However, in most cases, the explanations we offered would surely be modified by our current understanding. In addition, other effects have been discovered since. We will not attempt a recataloguing here, but instead will concentrate on one of the, by now, most well-established effects and will also discuss what has since become one of the most interesting phenomena.

There are very significant anomalies in the rate of high E_T jets (“cores”) in experiments such as Chacaltaya and Kanbala [43]. A QCD Monte Carlo was tuned to jet data at fixed target and collider energies (including the $Spp\bar{p}S$ and Tevatron). The prediction for χ_{12} , which is basically the product of the jets’ E_T and the jet-pair separation R_{12} , was then compared with the cosmic ray data. As shown in Fig. 27,

for energies above $\sqrt{s} \approx 5$ TeV (i.e. above the knee) the jet rate for $\chi_{12} \gtrsim 1000$ TeV.cm exceeds the QCD expectation by as much as two orders of magnitude. If we interpret this is an extension, to higher energies, of the large E_T jet excess observed at Fermilab, then it shows that there is an (orders of magnitude) increase of just the kind that we expect.

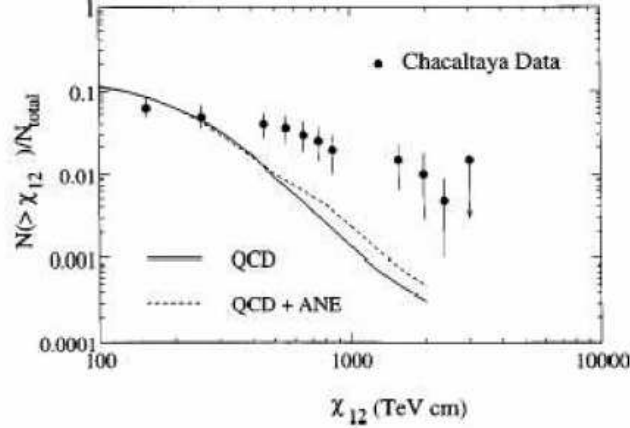


Fig. 27 Excess large E_T dijets (“cores”).

Ultra high-energy cosmic ray events, with $E_0 \gtrsim 10^{20}$ eV, have attracted great attention because the energy exceeds the GZK cut-off produced by the interaction of a proton with the cosmic background radiation. This suggests, of course, that the particles involved can not be protons. On the other hand, it is believed that the high velocities involved imply the particles must have traveled a long way and so should be stable. Within the Standard Model there is no other candidate besides the proton. As a result, both the origin and the nature, of the high-energy events is regarded as a mystery.

Within the sextet sector, there is an obvious candidate for producing the ultra high-energy events. Sextet neutrons are stable and will avoid the GZK cut-off, both because they are neutral and because they are massive. Also (because they have a large coupling to the pomeron) they will have a large high-energy hadronic cross-section. Clearly they could be responsible for the ultra high-energy cosmic rays. Indeed, they are probably responsible for an increasing fraction of the spectrum from energies lower than 10^{20} eV upwards. Since they would simply be very high energy dark matter, which is omnipresent in the universe, their origin would (presumably) not be a mystery.

To the extent that the existence of the ultra high-energy events is evidence for a stable, massive, particles that are strongly interacting (and preferably neutral), they could actually be regarded as evidence that dark matter is strongly interacting.

8. WHAT SHOULD BE SEEN AT THE LHC ?

Major evidence for the sextet sector, in the high luminosity mode of the LHC, will be the much larger than expected multiple vector boson and large E_T jet cross-sections discussed in the previous Section. Because large momentum longitudinal bosons (that preferentially decay to jet or lepton configurations with isolation problems) will be dominantly produced, the full size of the diboson cross-section may not be immediately recognized. Instead the major, observed, effect of this cross-section may be to contribute to the increased magnitude of large E_T jet cross-sections. Quite possibly, this increase will not be immediately identified as due to a sextet quark sector.

A priori, the neutral N_6 will also be quite difficult to detect, since missing energies of several hundred GeV will be common. The P_6 , assuming it is not too unstable, should be seen. Although a massive, charged, particle with a large production cross-section will surely cause much general interest, it also may not be immediately identified with the sextet sector. Instead, the double pomeron cross-section may well be the most definitive early evidence for the sextet sector.

8.1 Double Pomeron Exchange.

Vector bosons can be pair-produced directly in double pomeron exchange, via the sextet pion anomaly mechanism, as illustrated in Fig. 28.

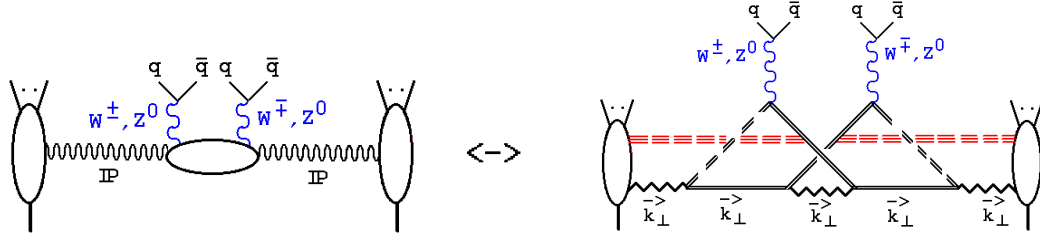


Fig. 28 Double pomeron production of W and Z pairs via sextet pions.

The kinematics needed for the derivation of this amplitude, as a straightforward extension of the argument of 5.2, are easily satisfied at the LHC. A parallel argument to that of 5.4 and 6.2 can then be used to obtain an order of magnitude estimate for the cross-section. The jet amplitude, analogous to Fig. 18(a), that has, apart from the anomaly loops, the same propagators and couplings as Fig. 28 is shown in Fig. 29(a). When the transverse momentum is electroweak scale, i.e. $|k_\perp| \gtrsim 100 GeV$, the cross-sections given by Fig. 28 and Fig. 29(a) are comparable. That is to say, at large k_\perp , the double pomeron production of W^+W^- and Z^0Z^0 pairs will give jet cross-sections that are as large as those predicted by standard QCD.

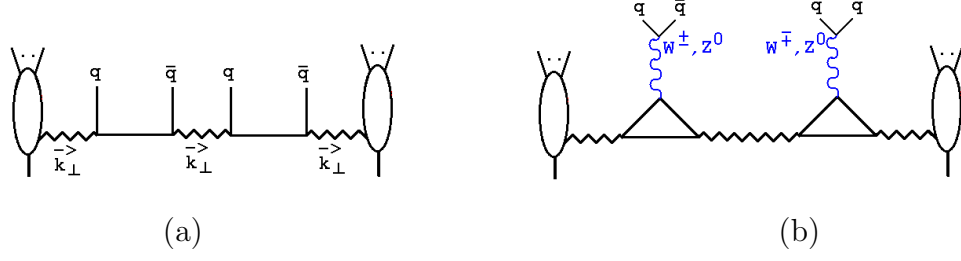


Fig. 29 (a) The comparable jet amplitude (b) a triplet sector amplitude

In Fig. 29(b) we show the lowest-order triplet sector amplitude that would comparably produce a vector boson pair decaying to jets, and would also involve the gluon exchanges necessary for pomeron exchange. Extending the argument of 5.4, since there are two sextet pions involved, and therefore two factors of F_{Π} , the cross-section given by Fig. 29(b) would be smaller by a factor of $\gtrsim O(10^{12})$.

Repeating the argument of 5.6 in the present context, the central double pomeron vertex of Fig. 28 should vary only slowly with k_{\perp} (with an electroweak scale), while the external hadron/pomeron vertices will have strong k_{\perp} - dependence and give a large increase as $|t|$ decreases. As was the case in our discussion of HERA events, we will obtain the maximum increase if the scattering protons are not diffractively excited. In this case, the increase will be given by the same product of hadron/pomeron couplings that is present in the elastic cross-section. When combined with a large $|t|$ amplitude that is larger than its triplet sector counterpart by $\gtrsim O(10^{12})$, this should imply a large double pomeron cross-section when $|t|$ is at the minimum kinematically allowed value, in agreement with the general argument of 7.1.

8.2 LHC Kinematics

If we consider the (symmetric) central region production of a state with mass $4M^2$ by colliding proton beams with momentum $\sqrt{S}/2$, then this corresponds to a minimum t value of

$$t \sim - \frac{4M^2 m_p^2}{S} \quad (8.1)$$

If we consider W^{\pm} (or Z^0) pair production then, in analogy with the double pomeron cross-section for pion pairs we might expect the maximal cross-section to be at $M \sim 2M_W \sim 170 \text{ GeV}$. In this case, with $\sqrt{S} = 14 \text{ TeV}$ and the proton mass set to 1 GeV , we obtain from (8.1)

$$t \sim -4 \left(\frac{0.17}{14} \right)^2 \sim -5 \times 10^{-4} \text{ GeV}^2 \quad (8.2)$$

which is close to the minimum value that is expected to be achieved by TOTEM in

the initial low luminosity running at the LHC. Therefore, it should be possible to detect the cross-section very close to it's maximal value.

If the CMS central detector is operational during the initial “soft physics” running period, then it should be straightforward to look for central W^\pm and Z^0 pairs, in combination with very forward scattered protons in the TOTEM Roman pots. The cross-section will be maximal when t is at it's minimum but should, of course, be observable over a range of t values. However, it will also be preferable to be as close as possible to threshold to minimize problems caused by the asymmetric decays of high momentum longitudinal vector bosons. In fact, with this in mind, it could be that at larger $|t|$ values multiple W^\pm and Z^0 pairs will be easier to detect because they are closer to threshold. Perhaps, since we expect the cross-sections to be so large, there could be spectacular events in which the far-forward protons are tagged and only (a multitude of) large E_T leptons are seen in the central detector!

A large double pomeron cross-section for W^\pm and Z^0 pairs immediately implies that the longitudinal components have direct strong interactions. Therefore, the observation of such a cross-section would be an immediate confirmation of the existence of the sextet sector and the sextet higgs mechanism. In addition, this cross-section can be looked for as soon as the LHC turns on. Consequently, we regard it as the top signature to be looked for as evidence for the sextet sector.

If we consider sextet neutrons and, to be appropriately above threshold, set $M = 1 \text{ TeV}$ in (8.1) we obtain a minimum $|t|$ value of

$$t \sim 4 \left(\frac{1}{14} \right)^2 \sim 2 \times 10^{-2} \text{ GeV}^2 \quad (8.3)$$

which will be detectable, if the cross-section is large enough. It would also be a spectacular process. The deflection of the tagged protons would determine that a very massive state was produced, while no charged particles would be seen in any of the detectors. Comparison with charged lepton production should allow a clear separation between this process and the multiple production of neutrinos by Z^0 's.

If the sextet nucleon double pomeron cross-section is extraordinarily large, it might be detectable in the low luminosity run of the LHC. If not, it might be seen by the high luminosity detector that will look for double pomeron production of the Standard Model Higgs particle.

8.3 Inclusive Cross-Sections for Sextet States.

As we noted in the previous Section, we expect cut-pomeron amplitudes of the form of Fig. 31(b) to be responsible for the inclusive production of mutiple vector bosons across most of the rapidity axis. This should be a major effect when the LHC is in high luminosity mode. However, as we already implied above, it is likely to take

time to determine that this phenomenon is indeed taking place, since the main effect will be the contribution to jet cross-sections. Note that since we showed above that the double pomeron production of jets via vector bosons will be comparable with the total jet rates that are expected, we would obviously expect the inclusive production of jets via vector bosons to be orders of magnitude larger (as we argued for, more generally, in the previous Section).

For the leptonic decays, the association of multiple leptons and missing E_t to multiple W 's will have obvious problems, which the close together decays of longitudinal bosons will only make worse. Multiple Z^0 states should be the easiest to detect, but the close together decays will also be a problem. Nevertheless, since the cross-sections should be so dramatically large, they should eventually provide emphatic evidence for the sextet sector.

If the N_6 and P_6^\pm pairs (and also η_6 pairs) are indeed too massive to be seen in double pomeron exchange, the central region inclusive cross-sections could (as we have already said) still be relatively large via cut-pomeron amplitudes. The problem then becomes how to detect such states.

8.4 Large Jet Cross-Sections and the Evolution of α_s

If the influence of the sextet sector on α_s is that the evolution stops at $E_T \sim m_t$, as we discussed in Section 6, then the LHC jet cross-sections will be further enhanced. Even according to conventional QCD predictions, the LHC jet cross-section persists for an order of magnitude in E_T beyond $E_T > m_t$ and so the lack of evolution would be straightforwardly evident, if it were the only phenomenon involved. In effect, Fig. 27, together with the large E_T jet excess at the Tevatron, are existing experimental evidence that the jet cross-section will be much larger than anticipated from conventional QCD, for almost all of the E_T range. If this enhancement is as big as we are anticipating, it will be very hard to imagine an alternative explanation besides the existence of the sextet quark sector.

ACKNOWLEDGEMENTS

I am grateful to Mike Albrow, Malcolm Derrick and Geoff Bodwin for valuable discussions

Appendix A. β -function Properties of QCD_S and $CSQCD_S$

A.1 The Infra-red Fixed-Point in QCD_S

We write the QCD_S β -function in the form

$$\beta(\alpha_s) = - \frac{g^4}{(4\pi)^2} \beta_0 - \frac{g^6}{(4\pi)^4} \beta_1 - \frac{g^8}{(4\pi)^6} \beta_2 + \dots \quad (A.1)$$

The three loop calculation of [44] gives, for n_f triplet flavors,

$$\beta_0 = 11 - \frac{2}{3}n_f, \quad \beta_1 = 102 - \frac{38}{3}n_f, \quad \beta_2 = \frac{2857}{2} - \frac{5033}{3}n_f + \frac{325}{54}n_f^2 \quad (A.2)$$

When $n_f = 6$, we obtain

$$\beta_0 = 7, \quad \beta_1 = 26. \quad (A.3)$$

When the two sextet flavors are included we obtain[44]

$$\beta_0 = 7 - 4T(R)n_f^6/3 = 7 - 4(\frac{5}{2})2/3 = 1/3, \quad (A.4)$$

and

$$\beta_1 = 26 - 20T(R)n_f^6 - 4C_2(R)T(R)n_f^6 = 26 - 100 - 66\frac{2}{3} = -140\frac{2}{3} \quad (A.5)$$

where $T(R) = C(R)/C(3) = 5/2$ and $C_2(R) = 10/3$ for sextet quarks. Therefore, QCD_S is (just) asymptotically-free and also has an infra-red fixed point at

$$\alpha_s \approx \frac{1}{34} \quad (A.6)$$

(There is a sense in which this can be argued to be present to all orders[45]). In addition, between the ultra-violet and infra-red fixed points the β -function remains very small ($< 10^{-6}$). As a result the massless theory evolves only very slowly and is almost scale-invariant.

A.2 Asymptotic Freedom in $CSQCD_S$

As in the body of the paper, we use $CSQCD_S$ to denote the “color superconducting” version of QCD_S obtained by adding a scalar field and using the usual higgs mechanism. (Note that, in this context, the “higgs mechanism” is a technical manipulation that has nothing to do with electroweak symmetry breaking.) It is a special property of QCD_S that a (complex) color-triplet Higgs scalar sector can be

added[46, 47] - with both the gauge-coupling *and* the Higgs self-coupling asymptotically free. We can illustrate this as follows.

Let $g(t)$ and $h(t)$ be the respective scale-dependent couplings, then

$$\frac{dg}{dt} = \beta(g, h) = -\frac{1}{2}b_0t^3 + \dots \quad (A.7)$$

where, now,

$$b_0 = \frac{1}{8\pi^2} \left[\beta_0 - \frac{1}{6} \right] \quad (A.8)$$

β_0 is calculated from the quark content, as above, and the $1/6$ is due to the triplet scalar. Similarly

$$\frac{dh}{dt} = \tilde{\beta}(g, h) = Ah^2 + Bg^2 + Cg^4 + \dots \quad (A.9)$$

where

$$A = \frac{7}{8\pi^2}, \quad B = -\frac{1}{\pi^2} \quad \text{and} \quad C = \frac{13}{48\pi^2}. \quad (A.10)$$

We can have $h \rightarrow 0$ consistently in (3.5) if $h = xg^2 + 0(g^3)$. This gives a stability equation for x , that is

$$\frac{dx}{dt} = g^2 (Ax^2 + B'x + C) \quad (A.11)$$

where $B' = B + b_0$. When the stability condition $(B')^2 > 4AC$ is satisfied there are two fixed-points of (3.7) and the smaller is stable for $t \rightarrow \infty$. The stability condition gives

$$(1 - \pi^2 b_0)^2 > \frac{91}{96} \quad (A.12)$$

which for b_0 small gives

$$\frac{5}{24} > 8\pi^2 b_0 \quad (A.13)$$

If there are 16 color triplet quarks, or six color triplets and two sextets, then

$$8\pi^2 b_0 = \frac{1}{6} < \frac{5}{24} \quad (A.14)$$

For comparison, if there are 15 color triplet quarks then

$$8\pi^2 b_0 = \frac{5}{6} > \frac{5}{24} \quad (A.15)$$

We conclude that, only when the number of quark flavors is “saturated”, as in QCD_S , can we use the Higgs mechanism to break the $SU(3)$ gauge symmetry to $SU(2)$, and so smoothly introduce a (single) massive vector into the theory, while *maintaining* the short-distance asymptotic freedom of the theory.

Appendix B. Properties of the Triangle Anomaly

In this Appendix we summarize the various properties of the triangle diagram that are used in the paper. We consider the contribution of the massless fermion loop, shown in Fig. B1,

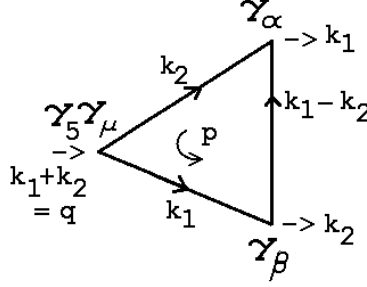


Fig. B1 The Fermion Loop Contribution to $T_{\mu\alpha\beta}(k_1, k_2)$

to an axial-vector/two-vector three current vertex, i.e.

$$\Gamma_{\mu\alpha\beta}(k_1, k_2) = \frac{i}{(2\pi)^4} \int \frac{d^4p \text{Tr}\{\gamma_5 \gamma_\mu (\not{k}_1 + \not{p}) \gamma_\alpha \not{p} \gamma_\beta (-\not{k}_2 + \not{p})\}}{p^2(k_1 + p)^2(p - k_2)^2}$$

A general decomposition of the symmetrized vertex

$$T_{\mu\alpha\beta}(k_1, k_2) = \Gamma_{\mu\alpha\beta}(k_1, k_2) + \Gamma_{\mu\beta\alpha}(k_2, k_1) \quad (B.1)$$

into invariant amplitudes is

$$\begin{aligned} T_{\mu\alpha\beta}(k_1, k_2) = & A_1 \epsilon_{\sigma\alpha\beta\mu} k_1^\sigma + A_2 \epsilon_{\sigma\alpha\beta\mu} k_2^\sigma + A_3 \epsilon_{\delta\sigma\alpha\mu} k_{1\beta} k_1^\delta k_2^\sigma \\ & + A_4 \epsilon_{\delta\sigma\alpha\mu} k_{2\beta} k_1^\delta k_2^\sigma + A_5 \epsilon_{\delta\sigma\beta\mu} k_{1\alpha} k_1^\delta k_2^\sigma + A_6 \epsilon_{\delta\sigma\beta\mu} k_{2\alpha} k_1^\delta k_2^\sigma \end{aligned} \quad (B.2)$$

with

$$\begin{aligned} A_1(k_1, k_2) &= -A_2(k_2, k_1) \\ A_3(k_1, k_2) &= -A_6(k_2, k_1) \\ A_4(k_1, k_2) &= -A_5(k_2, k_1) \end{aligned} \quad (B.3)$$

The large momentum region “anomaly” contribution to A_1 and A_2 gives

$$A_1 = \frac{1}{4\pi^2} + \dots, \quad A_2 = \frac{-1}{4\pi^2} + \dots, \quad (B.4)$$

leading to the “anomalous” divergence equation

$$(k_1 + k_2)^\mu T_{\mu\alpha\beta} = \frac{1}{2\pi^2} \epsilon_{\delta\sigma\alpha\beta} k_1^\delta k_2^\sigma \quad (B.5)$$

It is well-known[48] that (B.4) can be understood as the consequence of a large momentum shift of the Dirac sea, during the interaction, that does not conserve axial charge.

As is also well-known, the numerical value of (B.4) is fixed by requiring that the vector Ward identities hold, i.e.

$$k_1^\alpha \Gamma_{\mu\alpha\beta} = 0, \quad k_2^\beta \Gamma_{\mu\alpha\beta} = 0 \quad (B.6)$$

and so vector charge is conserved. For the invariant amplitudes A_i , the Ward identities require that

$$A_2 = k_1^2 A_5 + k_1 \cdot k_2 A_6 \quad (B.7)$$

and

$$A_1 = k_2^2 A_4 + k_1 \cdot k_2 A_3 \quad (B.8)$$

These identities imply, in turn, an inter-relation between the ultra-violet anomaly contribution and the infra-red structure of the other A_i . For example, when $k_1^2 = 0$, (B.7) becomes

$$A_2 = k_1 \cdot k_2 A_6 = \frac{q^2 - k_2^2}{2} A_6 \quad (B.9)$$

suggesting that there is a pole in A_6 . In particular, if we insert the ultra-violet anomaly term (B.4) into (B.9), we obtain

$$A_6 \underset{k_1^2 \rightarrow 0}{\sim} \frac{1}{2\pi^2 (k_2^2 - q^2)} + \dots \quad (B.10)$$

which appears to determine that, when $k_1^2 = 0$, there is a pole in A_6 at $k_2^2 = q^2$.

In fact, explicit expressions for the A_i can be given when $k_1^2 = 0$ (references to the original calculations can be found in [22]), i.e.

$$\begin{aligned} A_1 &= \frac{1}{4\pi^2} \left(\frac{k_2^2}{k_2^2 - q^2} \ln \frac{k_2^2}{q^2} + 1 \right) \\ A_2 &= \frac{1}{4\pi^2} \left(\frac{k_2^2}{k_2^2 - q^2} \ln \frac{k_2^2}{q^2} - 1 \right) \\ A_3 &= -A_6 = \frac{1}{2\pi^2} \frac{1}{k_2^2 - q^2} \left(\frac{k_2^2}{k_2^2 - q^2} \ln \frac{k_2^2}{q^2} - 1 \right) \end{aligned} \quad (B.11)$$

(While A_4 can be obtained from (B.8), A_5 is undetermined by (B.7) and is considerably more complicated.) Both (B.4) and (B.10) are clearly present in (B.11). However, it can easily be checked that there is no pole at $k_2^2 = q^2$ in A_6 . The logarithms of k_2^2 and q^2 are due to the “normal thresholds” in these channels, while the pole at $k_2^2 = q^2$ is a (triangle diagram) “anomalous threshold”. In general anomalous thresholds are hidden by normal thresholds. Consistent with this, the pole at $k_2^2 = q^2$ is present only if the expressions in (B.11) are continued to unphysical sheets of the logarithms.

In special kinematic configurations, the “anomaly pole” does appear on the physical sheet. In particular, with k_1^2 already set to zero,

$$k_2^2 = 0 \quad \implies \quad A_3 = -A_6 = \frac{1}{2\pi^2 q^2} \quad (B.12)$$

while

$$k_1 = 0 \equiv k_2^2 = q^2 \quad \implies \quad A_3 = -A_6 = \frac{1}{4\pi^2 q^2} \quad (B.13)$$

In both of these kinematic configurations the invariant functions containing the anomaly pole reduce to just the pole term with the residue determined entirely by the anomaly. In (B.13) the thresholds actually produce a partial cancelation of the pole. This partial cancelation is related to the property that, if q^2 is integrated over, the real part of the anomaly pole cancels and only the imaginary part δ -function remains. As we discuss in Section 2, this is important for the contribution of the U(1) anomaly in pomeron vertices.

If the massless fermions are actually confined, the anomaly pole can be interpreted as a Goldstone boson pole signaling chiral symmetry breaking. As we showed explicitly in [22], and briefly describe below, the pole is generated in the infra-red internal momentum region. Consequently, the Ward identities (B.7) and (B.8) involve a direct cancelation between the large internal momentum region generating anomaly contributions of the form (B.4) and the small internal momentum region giving the anomaly pole contribution. In effect, there are two distinct consequences of the presence of the ultra-violet anomaly (B.4). The first is the anomalous Ward identity (B.5). The second is that, for general momenta, the vector Ward identities require a cancelation between separate contributions (with different kinematic structure) from large and small internal momentum regions. If an internal large transverse momentum cut-off is introduced, (B.4) will be modified and the vector Ward identities will no longer hold. The contribution, to the vector current divergences of the anomaly pole terms will survive, however, since they are generated in the infra-red transverse momentum region[22].

If we keep just the anomaly pole contributions of A_3 and A_6 to $T_{\mu\alpha\beta}$ we can write

$$T_{\mu\alpha\beta}(k_1, k_2) = - \frac{1}{2\pi^2} \frac{(\epsilon_{\delta\sigma\alpha\mu} k_{1\beta} - \epsilon_{\delta\sigma\beta\mu} k_{2\alpha}) k_1^\delta k_2^\sigma}{(k_1 + k_2)^2} + \dots \quad (B.14)$$

This expression does not satisfy the vector Ward identities and does not have the axial current anomaly. When $k_1^2 = k_2^2 = 0$, and $q^2 \rightarrow 0$, we can rewrite (B.14) as

$$T_{\mu\alpha\beta}(k_1, k_2) \sim \frac{1}{2\pi^2} \frac{-q_\mu [\epsilon_{\delta\sigma\alpha\beta} k_1^\delta k_2^\sigma]}{q^2} \quad (B.15)$$

which now satisfies both vector Ward identities and also gives the anomalous divergence (B.5). We conclude that, by itself, the anomaly pole contribution violates the vector Ward identities, except at $k_1^2 = k_2^2 = 0$.

The ultra-violet anomaly contribution (B.4) is absent in (B.15) and yet the anomaly is present. To understand how the anomalous divergence can be due to the anomaly pole we must first discuss the internal momentum configuration that generates the pole. The analysis of [22] shows that, if external light-like momenta k^+ and k^- are directed as shown in Fig. B2, and p is the internal loop momentum, the pole is generated at $p = 0$.

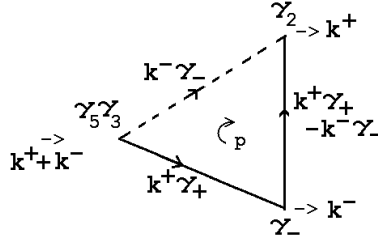


Fig. B2 Generation of the anomaly pole.

The γ matrices shown give an anomaly pole term

$$\Gamma_{32-} = - \frac{[\epsilon_{\sigma\delta 32} k_1^\sigma k_2^\delta] k_{1-}}{2\pi^2 q^2} = - \frac{k_+^2 k_-}{2\pi^2 q^2} \quad (B.16)$$

If $k^- \rightarrow 0$ then $q^2 = 2k^+ k^- \rightarrow 0$. The finite light-like momentum k^+ then flows along two of the internal lines while the third, the dashed line in Fig. B2, carries zero momentum. Because both poles of the zero momentum propagator participate in generating the anomaly pole, there is effectively a particle/antiparticle “chirality transition”, that is equivalent to an infra-red shift of the Dirac sea, during the interaction. This is how the anomaly pole produces an infra-red non-conservation of axial

charge that parallels that produced by the ultra-violet Dirac sea shift. The infra-red effect is present only when the fermions involved are massless and then only in the infra-red region where (B.15) is valid.

If the $1/q^2$ factor in (B.15) is to be interpreted as a Goldstone boson particle pole then q_μ must provide the coupling to the axial current while $[\epsilon_{\delta\sigma\alpha\beta}k_1^\delta k_2^\sigma]$ provides, potentially, a coupling to physical currents. There is a problem, however, in that k_1 and k_2 are both light-like and so $q^2 = 0$ implies that they are also parallel. Therefore, because of the ϵ -tensor, the pole residue vanishes, as is seen explicitly in (B.16). This should be expected, of course. Otherwise we would be able to obtain a coupling of a pion to finite momentum gluons. Nevertheless, we can avoid the vanishing of the pole residue if, as we go to the pole, we simultaneously go to an infinite-momentum frame. If we make a boost $a_3(\zeta)$ along the 3-axis and consider Γ_{32-} defined in the new frame, we can use either (B.15) or (B.16) to obtain

$$\Gamma_{32-} \sim \frac{k_+ \cosh \zeta [-k_+ k_- \sinh \zeta]}{\sqrt{2} q^2} \quad (B.17)$$

Since we still have $q^2 = 2k_+ k_-$, the limit $k_- \rightarrow 0$ again gives $q^2 \rightarrow 0$. However, the coupling $[k_+ k_- \sinh \zeta]$ is finite if $k_- \cosh \zeta$ is kept finite, i.e. if the mass-shell and infinite momentum limits are combined. As discussed in Section 2, the anomaly then provides a coupling to infinite momentum wee gluons. This is very important because, on general grounds, we expect to see wee-partons carry vacuum properties in the infinite momentum frame !!

Appendix C. The Multi-Regge Program

In this Appendix we provide a general description of the multi-regge program that we have formulated over the years which, as we note often in the main body of the paper, should ultimately provide the best framework for a complete derivation of the high-energy solution of QCD_S . We include some minimal historical background in order to explain the motivation for the program and to show why we have been led to connect QCD_S to the Critical Pomeron. More technical descriptions of the arguments we give can, for the most part, be found in our recent papers.

We will assume that the reader has a basic knowledge of reggeon diagrams. A review of elastic scattering diagrams and the transverse momentum kernels that appear in Section 2 can be found in Section IIIB of [22]. We will also make considerable use of multi-reggeon diagrams[49] that are the extension to multiparticle amplitudes of the elastic diagrams described in [22]. For our present purposes, it will be sufficient to understand firstly that, in the multi-reggeon diagrams, there are several distinct reggeon channels in which the elastic scattering kernels again appear - with all the same properties. Secondly, and very importantly, the vertices which couple the distinct reggeon channels contain anomalies that are not present in the (vector) gluon reggeon interactions appearing in elastic diagrams. We give details of these vertices, and the anomalies that occur, in the context of the discussion.

To begin with, we note that the asymptotic freedom of QCD almost certainly implies that total cross-sections must rise asymptotically if perturbation theory is to have any validity. The Critical Pomeron description of rising cross-sections was discovered[3] thirty years ago. While its derivation as a renormalization group solution of Reggeon Field Theory (RFT) implied that it satisfied full multiparticle t -channel unitarity[50, 51], it was soon established that it also satisfies all known s -channel unitarity constraints[52]. It remains today the only known rising cross-section solution of unitarity in the regge limit. In a sense, it is a fixed point solution of the regge limit (expressed in terms of physical degrees of freedom) analagous to the asymptotically-free fixed-point solution of the short-distance limit. The Critical Pomeron is, however, much more difficult to realize in a physical theory.

The critical solution of RFT was found via the well understood sub-critical theory (essentially the multiperipheral model plus unitarity corrections). The physical significance of the supercritical theory was the subject of much dispute and conflicting proposals were put forward. The solution we proposed[1, 2, 29] has the advantage that it is described by an explicit diagrammatic expansion that clearly satisfies reggeon unitarity. The supercritical diagrams are generated (as in a normal supercritical phase) by introducing a pomeron condensate in the critical RFT lagrangian. The condensate generates new classes of RFT diagrams, a simple example of which is

shown in Fig. C1. The two pomeron propagators produced by the condensate give k_{\perp} poles that have to be interpreted as particle poles, implying that there is a pomeron transition to a two vector reggeon state as shown.

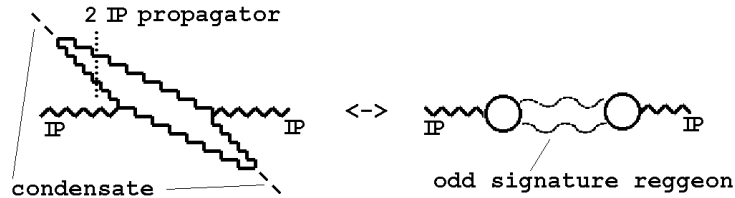


Fig. C1 A new RFT diagram generated by the pomeron condensate

Reggeon states involving many vector particle poles similarly appear in higher-order diagrams. Consequently, the RFT phase transition can be described by saying that divergences in rapidity produced in the subcritical graphical expansion (because the bare pomeron intercept is above one) are converted to vector particle divergences in k_{\perp} in the supercritical expansion. That is, the supercritical phase is characterized by the “deconfinement of a vector particle on the pomeron trajectory”.

We soon realized[2] that the deconfinement of a vector particle is exactly what should happen if it is possible to make a smooth transition from QCD to CSQCD, suggesting that the Critical Pomeron occurs, in particular circumstances, in QCD. It also suggested that a transition from perturbative reggeized gluon diagrams, describing a spontaneously-broken gauge theory, to non-perturbative pomeron diagrams describing a confining theory, could be followed within RFT. Confinement would have to be produced by the infra-red divergences of reggeized gluon diagrams.

We proposed[54], therefore, starting with the gluon and quark reggeon diagrams of QCD, but with the gauge symmetry completely broken so that all gluons are massive. The aim was to first restore the gauge symmetry to $SU(2)$, to obtain CSQCD, and to show that the diagrams obtained could be identified with those of supercritical pomeron RFT. We anticipated that infra-red divergences would produce confinement of $SU(2)$ color and a pomeron, while the broken part of the gauge group would provide the accompanying massive vector meson. Restoring the symmetry to $SU(3)$ would then be done within RFT and the result would be the Critical Pomeron. We gave arguments, based on complementarity, that with a transverse momentum cut-off imposed the symmetry restorations should take place smoothly and, over the years[49, 53], made a number of attempts to implement our proposal.

The derivation of our supercritical RFT solution involved many subtleties[29] that we eventually realized implied that the nature of the scattering hadron states has to be closely related to that of the pomeron. In particular, the “pomeron condensate” that defines the supercritical phase has to be associated with a (“wee parton”) component of the scattering hadrons. To derive the solution in a well-defined way,

it had proved necessary[29] to consider a multi-regge amplitude in which regge pole hadrons scatter via pomeron exchange. As a result we believed we should consider an analogous amplitude in QCD. That is, we should consider a “many-body” scattering amplitude, in an appropriate multi-regge region[49] of phase-space, in which regge pole pions and the pomeron could emerge together, as illustrated schematically in Fig. C2. Starting with the appropriate multi-regge perturbative reggeon diagrams, we would look for infra-red divergences that could produce pions and the pomeron as the gluons become massless. That, a priori, very complicated diagrams were to be considered is not as bad as it seems because the general structure of high-order diagrams is determined[49] from that of lower-order diagrams by reggeon unitarity.

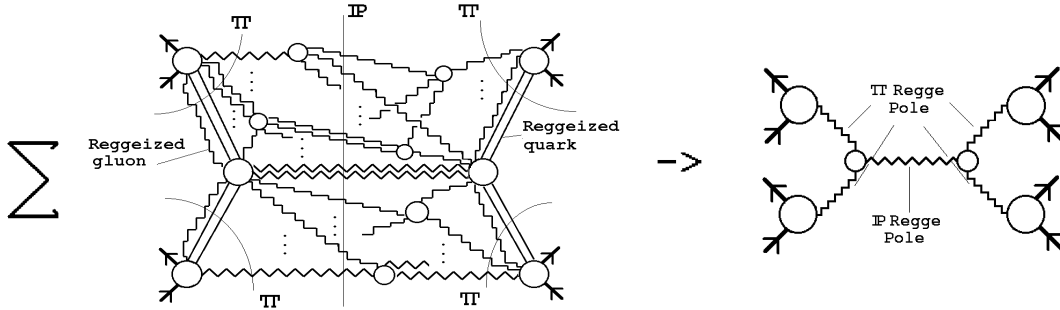


Fig. C2 The transition from perturbative reggeon diagrams to reggeized pions scattering via pomeron exchange.

In the sub-critical theory it was apparent that the criticality of the pomeron should depend on the number of hadron states and, therefore, on the number of quark flavors. Consequently, “saturating” the asymptotic freedom constraint, as in QCD_S , would be most likely to produce the critical behavior. The only physically realistic way to do this was[54] to add two sextet flavors and have the sextet higgs mechanism operative. It also became clear, rather quickly, that the special infra-red scaling properties of reggeon interaction kernels in QCD_S , which follow from the presence of an infra-red fixed-point, would have to be an essential ingredient of the infra-red divergence structure[54]. In addition there would have to be interactions (anomaly related?) to which divergences produced by the scaling properties would couple. Finally we realized that, because the Higgs mechanism scalar field is asymptotically free in $CSQCD_S$, restoration of $SU(3)$ color (which is to give the Critical Pomeron) can be carried out without a transverse momentum cut-off.

It soon seemed, therefore, that if Fig. C2 was to be implemented fully then, most likely, we would have to specifically consider QCD_S . There was, however, a major problem that, for a long time, prevented us from systematically developing a program to implement Fig. C2. If we consider QCD_S in isolation, then we can not find suitable external scattering states to provide a perturbatively well-defined starting amplitude within which pions and the pomeron could emerge as in Fig. C1.

Without this we can not determine, for sure, whether anomaly related divergences occur. Consequently, the anticipated mapping onto supercritical RFT can not be carried out. We initially supposed[54] that the external states could be multi-quark states. However, as will soon become clear, the pions and pomeron, that we are led to, do not couple to such states. In [49] we assumed the existence of external couplings with particular properties but, in this case, it was clear that the nature of the infra-red divergences that occurred depended on these assumptions.

Only recently[21, 22], have we understood that adding the electroweak vector boson sector of the Standard Model to QCD_S solves the problem of the external states for Fig. C2. As illustrated in Fig. C3, the desired pion amplitude should appear in a multi-regge limit[49] of an amplitude for multiple vector boson scattering.

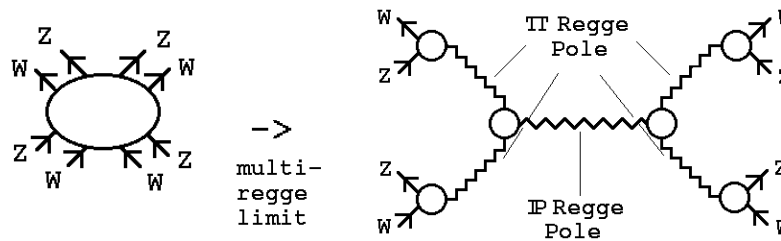


Fig. C3 The pion amplitude within a multiparticle vector boson amplitude.

Conversely, since W 's and Z 's have explicit perturbative couplings, this amplitude also has a perturbative reggeon diagram description. Most importantly for our program, because of the presence of elementary left-handed couplings, the perturbative reggeon vertices of the external W and Z states contain[21] anomalies that can give (with the cut-off manipulation that we discuss below) the infra-red divergences that we are looking for. We want, of course, to add the vector boson sector of the Standard Model to QCD_S in order to study the sextet higgs mechanism. Clearly, the fact that electroweak vector bosons provide the perfect external states for our multi-regge program could be related to the actual validity of the solution of QCD_S that we find. That is to say, our solution of QCD_S is effectively induced by the presence of the electroweak vector bosons and may, perhaps, only be valid in their presence[10].

For massless gluons, the individual reggeon diagrams in Fig. C1 have well-known infra-red divergences (that we will return to later) but, if the scattering states are color zero vector bosons, we expect that these divergences will cancel in the sum over all diagrams of a given order. Therefore, there must be an additional divergence phenomenon, if $CSQCD_S$ reggeon diagrams are to be mapped on to the pomeron diagrams of supercritical RFT via divergences. In fact, we now understand well that it is the appearance[22, 23] of chiral anomalies in, high order, multi-regge vertices that produces the divergences that we are looking for. The anomalies occur because these vertices contain triangle diagrams that result from the contraction (in the regge limit)

of larger loop feynman diagrams. Even though there are no axial vector currents in the elementary QCD interaction, γ_5 couplings are generated within these vertices by products of orthogonal γ -matrices.

We anticipate that, without a transverse momentum cut-off, the anomalies appear as a large transverse momentum phenomenon that produces (non-unitary) power enhancement of the high energy behavior. We have shown this explicitly in our analysis[21] of elastic vector boson scattering. The enhancement is avoided by the introduction of a cut-off but there is then a violation of gauge invariance Ward identities for the anomaly generating vertices (in analogy with our discussion of the elementary triangle diagram in Appendix B). As a result, as we discuss more explicitly below, infra-red transverse momentum divergences appear which couple directly to the part of the anomaly diagrams which, because the quarks involved are massless, contain the infra-red “anomaly pole”. (The anomaly pole contribution to a triangle diagram is discussed briefly in Appendix B and, at much greater length, in [22].) In effect, introducing a transverse momentum cut-off removes ultra-violet chirality violation produced by the anomaly and replaces it with infra-red chirality violation that produces anomaly poles. Since an anomaly pole can be interpreted as a Goldstone boson particle pole, this provides a crucial mechanism for a bound-state, Goldstone boson, spectrum to appear out of reggeon diagrams via infra-red divergences. Indeed, we will assume that anomaly poles survive higher-order corrections only when they are associated with a chiral symmetry.

Understanding that the infra-red divergence phenomenon that we are looking for should appear as a consequence of anomalies if a transverse momentum cut-off is imposed, the first step of our program is to look for this phenomenon within the multi-regge diagrams of $CSQCD_S$ obtained by setting the mass of an $SU(2)$ subgroup of gluons to zero. As described in Section 2, $CSQCD_S$ contains an $SU(2)$ triplet of massless (reggeized) gluons, plus two $SU(2)$ doublets and one singlet of massive (reggeized) gluons. The color symmetry breaking can be done, as we have already discussed, by adding a scalar field and using the usual Higgs mechanism (this is a technical manipulation that has nothing to do with electroweak symmetry breaking).

The main infra-red divergence of massless gluon reggeon diagrams is that associated with reggeization. Independently of the transverse momentum cut-off, this divergence exponentiates to zero all amplitudes with non-zero $SU(2)$ color (in the reggeon channel), while leaving finite color zero amplitudes. As described in more detail in [22], an infra-red fixed point implies that the interaction kernels of color zero massless gluons have a crucial infra-red scaling property (the ultra-violet version of which produces the leading-order BFKL pomeron). This scaling is an essential component of the anomaly related infra-red divergences that we are looking for, as we now discuss.

We consider reggeon states which contain both an $SU(2)$ color zero massless gluon component and an additional $SU(2)$ color zero component - either a massive gluon or a quark-antiquark pair. We consider the possibility of an infra-red divergence from the infra-red region where all the transverse momenta of the massless gluons scale uniformly to zero. If the massless gluons carry, overall, normal color parity ($=$ the signature) they will interact with the additional color zero component and, as a result, any divergence that occurs will be exponentiated via reggeization effects, giving a zero amplitude. If, however, the massless gluon component carries anomalous (\neq the signature) color parity the divergence will not exponentiate. This is because, as explained in [22], a gluon component of this kind can only couple to an anomaly vertex and anomalies can not occur in vector reggeon interactions that take place within a reggeon state. Consequently, the massless gluon component will have only self interactions, as illustrated in Fig. C4.

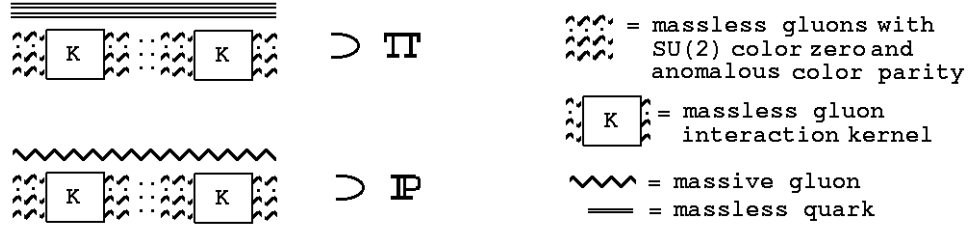


Fig. C4 Pomeron and pion reggeon states in $CSQCD_S$.

Provided there are external (to the reggeon state) anomaly vertices to which the complete reggeon states shown in Fig. C4 can couple the scaling property of the gluon self-interactions will produce a divergence (at zero transverse momentum for the gluons). The residue of this divergence contains a reggeon state that we can potentially identify as either a “pion” or a “pomeron”, as shown. If we can absorb this divergence into a “reggeon condensate”, this condensate will be an essential, zero transverse momentum, part of both the pion and the pomeron in $CSQCD_S$. Since “anomalous gluons” with $SU(2)$ color zero necessarily have odd signature (three is the minimal number), the pomeron given by Fig. C4 will be an even signature reggeon pole that is exchange degenerate with an odd signature, massive, gluon reggeon. This, together with the existence of a “pomeron condensate”, are crucial features of supercritical RFT. Also, since all amplitudes have $SU(2)$ color zero, if pion anomaly poles appear as we anticipate, we will have a spectrum with confinement and chiral symmetry breaking.

For the pion and pomeron to appear as in Fig. C4, via infra-red divergences, Fig. C2 has to be realized by the appearance of a “lowest-order” amplitude, of the form shown in Fig. C5, in which an anomaly that can couple the reggeon states appears in each vertex (as indicated by the A). The notation for Fig. C5 is the same

as that for Fig. C4 except that a new notation is introduced to indicate that each of the massless gluons now carries zero transverse momentum.

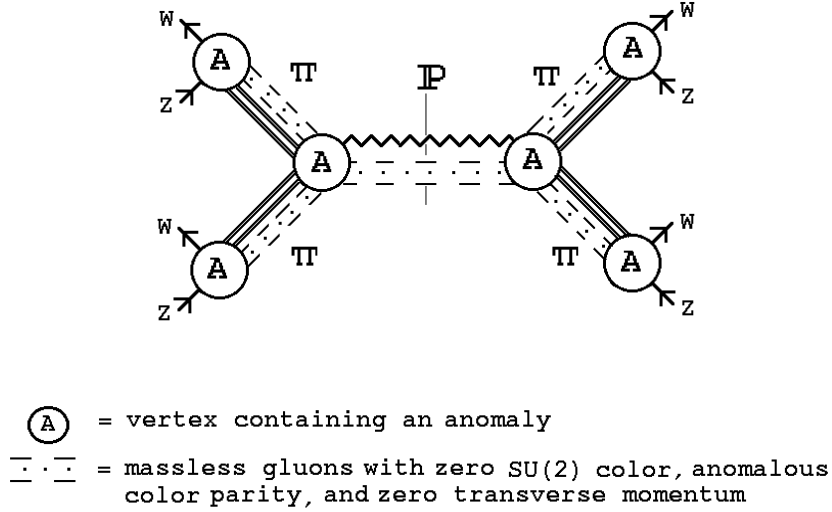


Fig. C5 Anomaly vertices that must appear in the pion amplitude.

The external anomaly vertices needed for Fig. C5 are identical to those that appear in our recent paper[21] deriving elastic scattering amplitudes of electroweak vector bosons. In that paper we demonstrated that anomalous color parity gluons have the needed coupling. In the elastic scattering context, it is very clear how the use of a cut-off removes bad, large transverse momentum based, high-energy behavior produced by the anomalies and, instead, introduces anomaly dominated infra-red divergences that potentially produce “non-perturbative” anomaly pole Goldstone bosons. Although we did not discuss the generation of the anomaly pole explicitly in [21], we did give a brief summary of how the anticipated infra-red divergences should be mapped onto RFT and the amplitude for pion exchange obtained.

The anomaly vertices obtained in [21] contain triangle diagrams resulting from the contraction of larger loop feynman diagrams just as illustrated in Fig. 2. As described in Appendix B, an anomaly pole is generated in the triangle diagram by a zero momentum quark line (the partially broken line in Fig. 2). It is important that, as illustrated in Fig. 2, it is the longitudinal polarization of the on-shell massive vector boson that produces the quark/antiquark coupling in the anomaly triangle diagram. (Note that, in the calculation of [21], the on-shell massive gluon in Fig. 2 was replaced by a massive electroweak vector boson.)

The anomaly that occurs in diagrams that contribute to the pion/pion/pomeron vertex in Fig. C5 is discussed in [23] and [55]. The reduction to a triangle diagram is as illustrated in Fig. C6 and it is the U(1) anomaly that is involved.

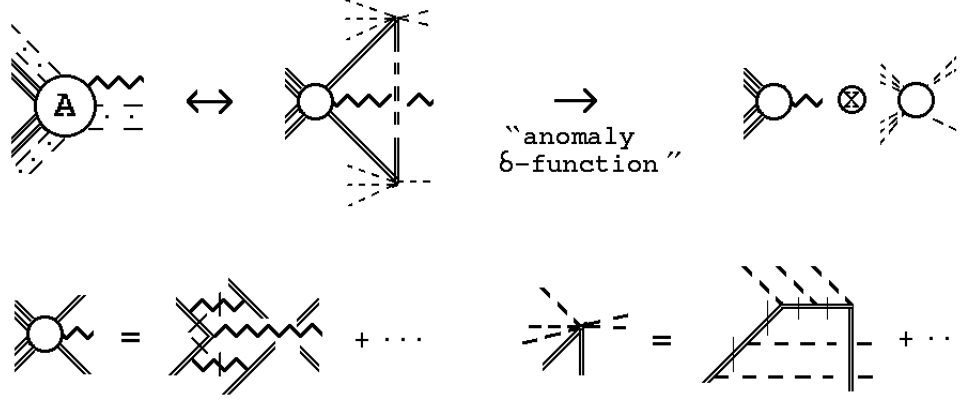


Fig. C6 The reduction to a triangle diagram that involves the U(1) anomaly.

(The notation is the same as in previous diagrams.) The anomaly pole is present but, because it is integrated over, it contributes as an “anomaly δ -function” and plays the remarkable role, also illustrated in Fig. C6, that it factorizes off the (zero transverse momentum) anomalous gluon interaction from the remaining “hard interaction”. The anomaly δ -function is again generated by a zero momentum quark line (illustrated by a broken line in Fig. C6) which undergoes a chirality transition. The hard interaction production of a massive gluon has an overall axial vector nature that compensates for this transition. To produce the axial coupling it is essential that the exchanged on-shell massive gluons within the hard interaction are longitudinal. (It is also important that these gluons carry zero light-cone momentum in a frame in which the pion carries finite light-cone momentum.)

Because each of the external reduced triangle diagrams that we have discussed contain anomaly contributions, imposing a transverse momentum cut-off will lead to a violation of Ward identities for the gluons coupling to such vertices. A scaling transverse momentum divergence should then appear in each pion channel and generate Fig. C5, as we have discussed above. We anticipate that there will be an overall logarithmic divergence as the transverse momenta in all channels are scaled uniformly to zero and that this is what we will have to factorize off to obtain the physical amplitude. However, to be sure of this and to elaborate the divergence phenomenon in full requires more details of the calculation than we presently have. We have, so far, carried out the full analysis only in the situation described in [22] in which we used the pion anomaly pole approximation that we describe in Section 2.

For the more general case of the reggeized pion amplitude appearing in Fig. C5, we can say the following. The divergence is at zero transverse momentum, which (in an appropriate frame) should be equivalent to zero four momentum for the gluon vertex of the effective triangle diagram in Fig. 2. From (B.13), we see that in this kinematic configuration the triangle diagram amplitude reduces to a “pion” anomaly pole, as illustrated in Fig. 2. Thus, as we have anticipated, the anomaly pole should

provide the mechanism whereby a pion particle pole appears (in the residue of the infra-red divergence) as part of the pion reggeon state.

To obtain the multi-regge amplitudes of QCD_S from those of $CSQCD_S$, via RFT, it is clearly necessary to understand in complete detail how the full set of divergent $CSQCD_S$ diagrams maps onto super-critical RFT. In higher-orders we expect to find vertices, of the form shown in Fig. 10, in which massive gluons are produced by a wee gluon interaction only. Interactions of this kind should lead to particle pole interactions within pomeron vertices, just as is produced by the pomeron condensate in the supercritical pomeron phase[29].

Although there is every indication that the reggeon diagrams of $CSQCD_S$ can be mapped onto supercritical RFT, it remains a major challenge to carry out the mapping in full. Our hope is that the (relative) simplicity of the external vector boson couplings, appearing in Fig. 2, will finally make it feasible. It also remains to be determined how a pion anomaly pole, which occurs at zero transverse momentum, combines with reggeization at spacelike momentum transfer. In the anomaly pole vertex method[22], that we use in Section 2, we effectively assume that the on-shell pion couplings can be obtained by an anomaly pole coupling of the form shown in Fig. 2. While the above discussion suggests that this should be a straightforward outcome of the full multi-regge calculation, it remains to be shown.

With the mapping of $CSQCD_S$ onto supercritical RFT established, it should be straightforward to show that the high-energy behavior of QCD_S is that of the Critical Pomeron. Critical Pomeron amplitudes can be, and have been, calculated[52] without reference to QCD. There will, however, be much to understand about the limiting process involved, particularly with respect to the formation of baryons. For our present purposes we have, in Sections 2 and 3, concentrated on the underlying physical phenomenon which describes the pomeron in QCD_S .

References

- [1] A. R. White, “The Reggeon Field Theory Beyond the Critical Point ...”, CERN Preprint TH.2259, January, 1977.
- [2] A. R. White, Proceedings of the Int. Conf. on High Energy Physics, Tokyo (1978).
- [3] A. A. Migdal, A. M. Polyakov and K. A. Ter-Martirosyan, *Zh. Eksp. Teor. Fiz.* **67**, 84 (1974); H. D. I. Abarbanel and J. B. Bronzan, *Phys. Rev.* **D9**, 2397 (1974).
- [4] W. J. Marciano, *Phys. Rev.* **D21**, 2425 (1980).
- [5] E. Braaten, A. R. White and C. R. Willcox, *Int. J. Mod. Phys.*, **A1**, 693 (1986).
- [6] A. R. White, “Sextet Quark Physics at the Tevatron? ”, hep-ph/0405190.
- [7] A. R. White, “The Sextet Higgs Mechanism and the Pomeron ”. Presented at ISMD 2004 - hep-ph/0409181.
- [8] M. G. Albrow, “The White Pomeron, Color Sextet Quarks and Cosmic Ray Anomalies”. Presented at the Workshop on QCD and Cosmic Physics, Erice, 2004 - hep-ph/0409308.
- [9] K. Kang and A. R. White, *Int. J. Mod. Phys.* **A2**, 409 (1987).
- [10] A. R. White, Contributions to XVIIth Rencontre de Blois and Gribov-75 - to appear.
- [11] V. S. Fadin, E. A. Kuraev and L. N. Lipatov, *Sov. Phys. JETP* **45**, 199 (1977); V. S. Fadin and L. N. Lipatov, *Nucl. Phys.* **B406**, *Nucl. Phys.* **B477**, 767 (1996) and further references therein.
- [12] J. B. Bronzan and R. L. Sugar, *Phys. Rev.* **D17**, 585 (1978), this paper organizes into reggeon diagrams the results from H. Cheng and C. Y. Lo, *Phys. Rev.* **D13**, 1131 (1976), **D15**, 2959 (1977).
- [13] V. S. Fadin and V. E. Sherman, *Sov. Phys. JETP* **45**, 861 (1978).
- [14] J. Bartels, *Z. Phys.* **C60**, 471 (1993) and further references therein.
- [15] R. Kirschner, *Nucl. Phys. Proc. Suppl.* **51C**, 118 (1996).
- [16] A. R. White, *J. Mod. Phys.* **A8**, 4755 (1993).
- [17] C. Ewerz, “The Perturbative Pomeron and the Odderon: Where Can We Find Them?” hep-ph/0403051.

- [18] A. R. White, Proceedings of the 8th International Symposium on Very High Energy Cosmic Ray Interactions, Tokyo (1994).
- [19] A. R. White, hep-ph/9704248 (1997)
- [20] T. E. Clark, C. N. Leung, S. T. Love and J. L. Rosner, *Phys. Lett.* **B177**, 413 (1986).
- [21] A. R. White, *Phys. Rev.* **D69**, 096002 (2004).
- [22] A. R. White, *Phys. Rev.* **D66**, 056007 (2002).
- [23] A. R. White, *Phys. Rev.* **D66**, 045009 (2002).
- [24] V. N. Gribov, *Nucl. Phys.* **B139**, 1 (1978), S. Mandelstam, *Phys. Rev.* **D19**, 2391 (1978).
- [25] Y. Iwasaki, K. Kanaya, S. Kaya, S. Sakai, T. Yoshie, *Phys. Rev.* **D69**, 014507 (2004).
- [26] A. Armoni, M. Shifman and G. Veneziano, hep-th/0403071.
- [27] ZEUS Collaboration (M. Derrick et al.), *Z. Phys.* **C74** 207 (1997).
- [28] J. B. Kogut, M. A. Stephanov, D. Toublan, J. J. M. Verbaarschot and A. Zhitnitsky, *Nucl. Phys.* **B582**, 477 (2000).
- [29] A. R. White, *Int. J. Mod. Phys.* **A11**, 1859 (1991).
- [30] A. R. White, *Phys. Rev.* **D29**, 1435 (1984) and references therein.
- [31] For details of Gribov's confinement picture and for references to the original papers see Y. L. Dokshitzer and D. E. Kharzeev, hep-ph/0404216 (2004).
- [32] ZEUS Collaboration (S. Chekanov et al.), hep-ex/0401003.
- [33] H1 Collaboration (C. Adloff et al.), *Eur. Phys. J.* **C30**, 1 (2003).
- [34] S. Bentvelsen, J. Engelen and P. Kooijman, Physics at Hera, Vol. 1, 23.
- [35] H1 Collaboration (C. Adloff et al.), *Z. Phys.* **C74** 191 (1997).
- [36] G. E. Forden, presentation at ISMD94. See also D0 Collaboration (S. Abachi et al.). FERMILAB-CONF-95-218-E (1995), presented at HEP 95.
- [37] UA1 Collaboration (C. Albajar et al.), *Phys. Lett.* **B193** 389 (1987).

- [38] CDF Collaboration (T. Affolder et al.), *Phys. Rev. Lett.* **88** 042001 (2002).
- [39] CDF Collaboration, “CDF-QCD Group Run 2 Results” - <http://www-cdf.fnal.gov/physics/new/qcd/inclusive/index.html>.
- [40] See S. I. Nikolsky, *Phys. Atom. Nucl.* **62**, 2048 (1999), for references.
- [41] D. Kazanas and A. Nicolaidis, *Gen. Rel. Grav.* **35**, 1117 (2003) - hep-ph/0109247; “Cosmic Ray Spectrum ”Knee”: A Herald of New Physics?” - astro-ph/0103147.
- [42] S. Barshay and G. Kreyerhoff, *Mod. Phys. Lett.* **A16**, 1061 (2001).
- [43] Z. Cao, L. K. Ding, Q. Q. Zhu, Y. D. He, *Phys. Rev.* **D56** 7361 (1997).
- [44] O. V. Tarasov, A. A. Vladimirov and A. Yu. Zharkov, *Phys. Lett.* **B93**, 429 (1980).
- [45] T. Banks and A. Zaks, *Nucl. Phys.* **B196**, 189 (1982).
- [46] D. J. Gross and F. Wilczek, *Phys. Rev.* **D8**, 3633 (1973).
- [47] T. P. Cheng, E. Eichten and L. F. Li, *Phys. Rev.* **D9**, 2259 (1974).
- [48] V. N. Gribov, “Gauge Theories and Quark Confinement”, published by PHASIS Research and Publishing Corporation, Moscow (2002).
- [49] A. R. White, *Phys. Rev.* **D58**, 074008 (1998). This paper describes all the necessary multi-regge limits, as well as the construction of multi-reggeon diagrams via reggeon unitarity.
- [50] V. N. Gribov, I. Ya. Pomeranchuk and K. A. Ter-Martirosyan, *Phys. Rev.* **139B**, 184 (1965).
- [51] A. R. White, “The Past and Future of S-Matrix Theory”, published in “Scattering”, edited by E. R. Pike and P. Sabatier (Academic Press, 2002).
- [52] M. Moshe, *Phys. Rept.* **37**, 255 (1978).
- [53] A. R. White, *Nucl.Phys.Proc.Suppl.* **96**, 277 (2001).
- [54] A. R. White, CERN preprint TH.2976 (1980) - a summary of this paper is presented in the Proceedings of the XVIth Rencontre de Moriond, Vol. 2 (1981).
- [55] A. R. White, *Phys. Rev.* **D63**, 016007 (2001).